Harmonic Spectra Analysis of Digital SPWM in VSI With DC Bus Ripple and Dead-Time Effects

Haozhe Wang, Jinbang Xu, Jie Ye, Baojin Li, Songtao Huang, *Student Member, IEEE*, Yukai Huang, Dong Liu, and Anwen Shen, *Member, IEEE*

***Abstract*—This article presents a closed-form analytical solution to the harmonic spectrum of output voltage of a single-phase H-bridge inverter, and gives the precise harmonic spectrum considering the effects of dead time and dc bus voltage ripple in a digitally controlled system. Since the H-bridge is the basic block in converters, this solution and spectrum can be extended and applied to a variety of pulsewidth-modulation-based topologies. The interaction between modulation waveform and triangular during the modulation process is fully analyzed from a mathematical perspective so that the combined effects of digital sampling, dead time, and dc bus voltage ripple on the output voltage are summarized in time and frequency domains. Furthermore, the presented harmonic spectra do not need to judge the current polarity in calculation, which means that the exact amplitude and phase of each output harmonic can be obtained accurately, providing the important theoretical basis for system parameter design and specific harmonic compensation or elimination. The presented analysis results are verified by simulations and experiments.**

***Index Terms*—DC bus ripple, dead time, digital sinusoidal pulsewidth modulation (DSPWM), double fourier series, harmonic analysis, voltage source inverter (VSI).**

I. Introduction

DUE to appealing advantages such as a high-input power factor, sinusoidal output, and bidirectional power flow capability [1], [2], [3], voltage-source inverters (VSIs) with controllers have been widely used in industrial applications in recent years, especially in high-voltage direct current transmission systems, motor drives, and grid integration of renewable energies [4], [5], [6]. Carrier-based pulsewidth modulation (PWM) schemes are commonly applied in VSIs to synthesize the required power supplies through power semiconductor devices [7], [8], but the output voltage is square wave containing undesired high-frequency harmonic components related to carrier frequency, while the nonlinear factors in the modulation process introduce undesired low-frequency harmonic components, causing grid distortion and reducing the power quality. To protect the power grid and improve the performance of VSI, the output harmonic components of the converter need to be eliminated or compensated, and the accurate detection of harmonic components is a premise, therefore, the analysis of the undesirable harmonic components as well as the output voltage harmonic spectrum is necessary.

The controllers in VSI systems can be divided into two types: analog and digital; and the digital controller is preferred in modern power systems due to its benefits of flexible operation, easy calculation and control, strong reliability and antiinterference, low cost, and so on [9], [10], [11], [12]. In the low-frequency modulation process, the digital controller, especially that of high speed, can be equivalent to the analog controller; however, due to the limitation of switching frequency, the high-frequency modulation process of the digital controller is quite different from that of the analog controller.

A portion of present analysis of PWM harmonic spectrum assumes that the semiconductor switch is ideal, i.e., the switch operates instantaneously, which cannot be achieved in practice [13], [14], [15]. The actual semiconductor device has a nonzero switching duration, which means that it takes time to turn ON or OFF. To avoid both transistors of the same branch conduct simultaneously, and thus, shoot-circuit, the dead time is introduced to delay the low-to-high transitions in the gating signals of each transistor by Δt.

Another common assumption in analyzing the harmonic spectrum is to consider the dc bus voltage in the converter as ideal, which means that the dc bus voltage contains only a pure dc component [16], [17]. However, in the practical applications, especially when the dc bus is a floating capacitor, the dc bus tends to generate a large amount of low-frequency harmonic components, meaning that the dc bus voltage oscillations are inevitable.

The high-frequency harmonic components in the dc bus ripple can be easily suppressed, but the elimination of low-frequency harmonic components requires a large capacitance, leading to an increase in the cost and size of the system. In general, a small ripple (less than 10%) in the dc bus voltage is acceptable. Therefore, if the dc bus is simply analyzed and modeled as ideally constant, the unanticipated harmonic components will be introduced to the output voltage as well as PWM waveform by the ripple in the dc bus voltage, thus resulting in distortions.

Manuscript received 12 September 2022; revised 13 December 2022, 6 February 2023, and 24 March 2023; accepted 28 April 2023. Date of publication 2 May 2023; date of current version 21 June 2023. This work was supported by the Natural Science Foundation of China under Grant 62173156. Recommended for publication by Associate Editor D. O Neacsu. *(Corresponding author: Jie Ye.)*

The authors are with the National Key Laboratory of Science and Technology on Multispectral Information Processing and the Key Laboratory of Image Processing and Intelligent Control, School of Artificial Intelligence and Automation, Huazhong University of Science and Technology, Wuhan 430074, China (e-mail: wanghaozhe@hust.edu.cn; xujinbang@mail.hust.edu.cn; yejie_hust@hust.edu.cn; d201880675@hust.edu.cn; songtao_huang@hust.edu.cn; hyk_aia@hust.edu.cn; m202072704@hust.edu.cn; sawyi@mail.hust.edu.cn).

Color versions of one or more figures in this article are available at https://doi.org/10.1109/TPEL.2023.3272381.

Digital Object Identifier 10.1109/TPEL.2023.3272381

The three aforementioned nonlinear factors, digitization, dead time, and dc bus voltage ripple, are superimposed on each other and affect the harmonic distribution and total harmonic distortion (THD) of output voltage in the actual system. Harmonic components bring problems such as reduced power quality and poor system stability, preventing the power converters from following strict power quality constraints.

The modulation theory has been a major research area in power electronics for decades, and different approaches have been proposed to analyze the harmonic content of carrier-based modulation schemes. The double Fourier series approach has been introduced for the analytic determination of inverter harmonic content in [18]. Then, [19] and [20] transformed the classic 2-D Fourier series as well as harmonic spectrum into a 1-D form by superposition. Another approach to obtain the harmonic content is to combine a time-domain simulation of PWM waveform with the fast Fourier transform (FFT) technique, thus replacing the complex mathematical analysis. The major drawback of this approach is that it requires a sufficiently small simulation time step to lower the noise floor for any meaningful conclusions [21], [22], [23].

The analytical solutions derived from the double Fourier series are not only intuitive but also provide accurate harmonic spectra, enabling the precise comparison of different modulation strategies down to each harmonic, while providing the theoretical basis for harmonic cancellation. Therefore, the analysis approach based on the double Fourier series is essential and has become the basis for most further modulation research [24], [25], [26].

The double Fourier series approach has gained numerous extensions. Holmes and Lipo in [27] analyzed different variations of the PWM process in power converters and gave the expression of output harmonic components. The authors in [28] and [29] turned to the digital control system and studied the nonlinear effect of digitization and sampling on output voltage. The authors in [30], [31], and [32] introduced another nonlinear factor dead time to make the analysis more practical, giving the harmonic spectrum under the assumption that the output current polarity is known. However, the aforementioned harmonic analyses optimistically assume that the dc bus voltage contains only a fixed dc component and is free of oscillations.

Recent studies have focused on the impact of nonideal dc bus voltage on power converters. The authors in [33] and [34] concern the influence of the dc bus voltage ripple and propose different compensation methods, but do not describe the mechanism of this influence in detail. The authors in [35] consider only the second-order harmonic in floating capacitor voltage and give the mathematical expressions for output harmonic spectrum in the cascaded H-bridge converter. The expressions for the output voltage spectrum of a half-bridge VSI with and without dc bus compensation are given in [36] and [37], respectively, but these expressions are based on natural sampling and contain a switching function, which differ from practical applications. While concentrating on the dc bus ripple, these studies ignored the effects of other nonlinear factors such as dead time.

TABLE I
COMPARISON OF RESEARCH CONTENTS

	Combined nonlinear factors		
	Digitization	**Dead−time**	**DC bus ripple**
[27]	×	×	×
[28] − [29]	✓	×	×
[30] − [32]	✓	✓	×
[33] − [37]	×	×	✓
This Article	✓	✓	✓

The superposition of all typical nonlinear factors for combined studies is challenging—the superposition of multiple nonlinear factors, especially the superposition of dead time and dc bus voltage ripple, will make the harmonic analysis and calculation process extremely complex; it will also make the pattern of output harmonic distribution not obvious.

Therefore, the current harmonic analyses only highlight the impacts of certain types of nonlinear factors on the system, without fully considering all nonlinear factors that have significant effects on the system, and idealizing some of the conditions will make their conclusions differ from practical applications.

In this article, the generation mechanism of output voltage harmonic components in modulation process is analyzed with fully considering the impacts of all typical nonlinear factors in modern digitally controlled VSIs, and a general and well-established harmonic analytical solution that can accurately determine the actual harmonic spectrum is proposed.

By applying this analysis method step by step, this article first analyzes the effects of each nonlinear factor when acting individually, then analyzes the superimposed impacts by combining two different factors, and finally, models the actual system by combining all the typical nonlinear factors and analyzes their superimposed effects. Thus, the qualitative conclusions are given about the effects of introducing different nonlinear factors to the system, either individually or in combination.

The comparison between the research contents of this article and the published articles using double Fourier series for harmonic analysis is shown in Table I.

With the proposed analytical solution, the detailed analytical harmonic spectrum of the single-phase H-bridge inverter output voltage that considers the superimposed effects of digitization, dead time, and dc bus voltage ripple is derived for the first time, and the computable expression with high precision for the phase and amplitude of each harmonic is obtained from this spectrum.

Ultimately, this article gives clear quantitative conclusions about the effects of these nonlinear factors on the output harmonic components, both individually and in combination, through this accurate and analytical harmonic spectrum.

The proposed analytical solution is suitable for harmonic analysis in different cases, and the derived harmonic spectra and computable expressions are of guidance for harmonic compensation and system parameter design, such as calculation of optimal dead time; design of more efficient control and filter parameters or precise elimination of specific harmonic

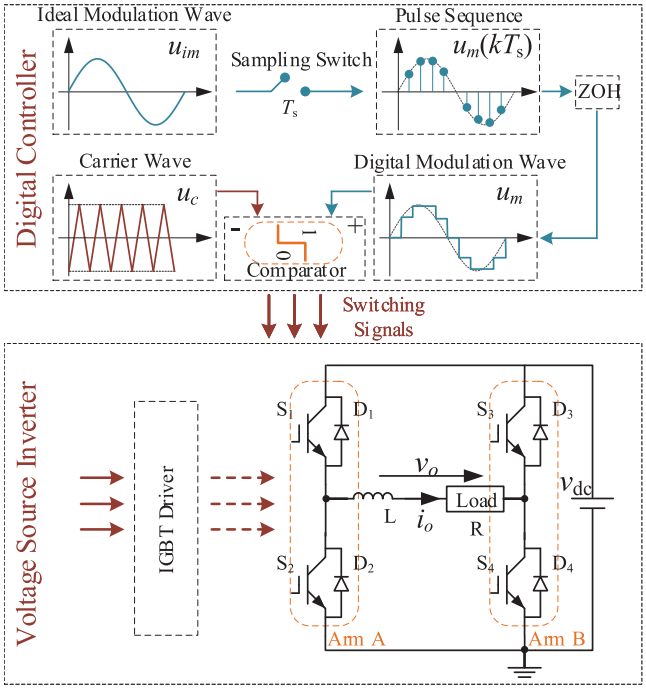

Fig. 1. Diagram of the carrier-based PWM single-phase VSI structure in the digital control system.

components using inverse compensation with the accurate amplitude and phase of each harmonic is known.

Noteworthy, the proposed harmonic analysis method and derived results are quite scalable and can be easily extended in a similar manner to the vast variety of structures, modulation strategies, phase numbers, and other situations.

The results in this article, especially the general harmonic analysis method, analytical harmonic spectra, and high-precision computable expressions that consider all the typical nonlinear factors, are not covered in previous literature and are verified by both simulations and experiments.

The rest of this article is organized as follows. Section II builds a model of digitally controlled single-phase H-bridge VSI, and qualitatively analyzes the effects of nonlinear factors during bipolar modulation in time domain. Section III develops a general harmonic analysis method and presents the well-established expressions and harmonic spectra of output voltage under different conditions while the dc bus voltage is considered as a constant. The analyses in Section IV are extended to the dc bus with considerable voltage ripple. Section V gives quantitative conclusions on the effects of nonlinear factors. Section VI provides the verifications in experiments. Finally, Section VII concludes this article.

II. Modeling of the Inverter and Analysis of Nonlinear Factors

Fig. 1 shows the diagram of the H-bridge voltage source inverter in a digital control system. The single-phase H-bridge consists of two arms (Arms A and B) with four transistors (S_1, S_2, S_3, S_4) and their antiparallel diodes (D_1, D_2, D_3, D_4), which provide the current loop. The switching signals of transistors are obtained by logically comparing the modulation waveform u_m with the triangular carrier u_c in the controller. In addition, the proposed analysis method is applicable to all switching tubes, and the IGBT in Fig. 1 is only used as an example.

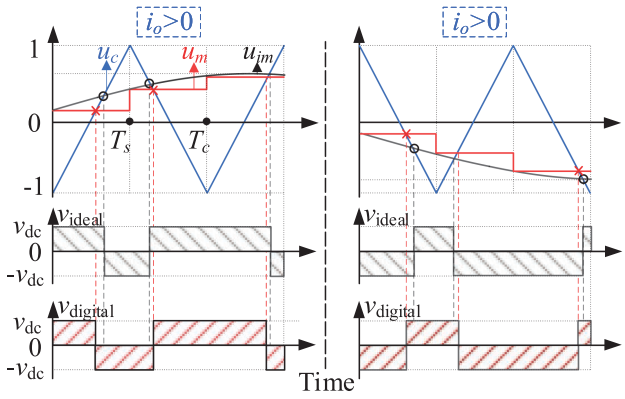

Fig. 2. Effect of digital PWM on output voltage in time domain.

Among the modulation strategies, bipolar modulation is chosen in this article, whose output is only two levels, the modulation process is easy to analyze, and the output harmonic distribution pattern is typical. Most importantly, since the analysis method under bipolar modulation can be easily extended to other arbitrary modulation strategies, it can be applied as the basis for harmonic analysis.

During the bipolar modulation process, when the amplitude of modulation waveform is higher than the carrier, the controller gives the switching signals to turn S_1 and S_4 ON and S_2 and S_3 OFF, providing an output voltage with a positive dc bus voltage ($v_o = v_{dc}$); in the other case, the switching state of the transistors and the polarity of the output voltage are reversed ($v_o = -v_{dc}$). Consequently, the output voltage represents a pulse train whose pulsewidth depends on the value of the modulation waveform, i.e., the PWM.

In digital control systems, data need to be sampled and computed, so the modulation waveform cannot be generated in real time and there is a delay compared to analog systems, whose effect is more obvious for low-speed controllers, as it can be compensated easier in some applications with high-speed controllers such as FPGA or suitable predictive models.

In brief, the digitized modulation waveform u_m is obtained by sampling and holding from an ideal modulation waveform u_{im}, as shown in Fig. 1. As can be seen in Fig. 2, the intersections of u_m and the triangular carrier u_c have changed relative to u_{im}, which shifts the output voltage in the time domain and brings a nonlinear effect to the digital system.

Besides, the semiconductor switches in the practical inverter system cannot be considered ideal; they need turn ON time t_{on} and turn OFF time t_{off} to turn ON and turn OFF, respectively. Therefore, the dead time Δt is required to be introduced into the switching signals to avoid the simultaneous conduction of the two switch devices of the same arm.

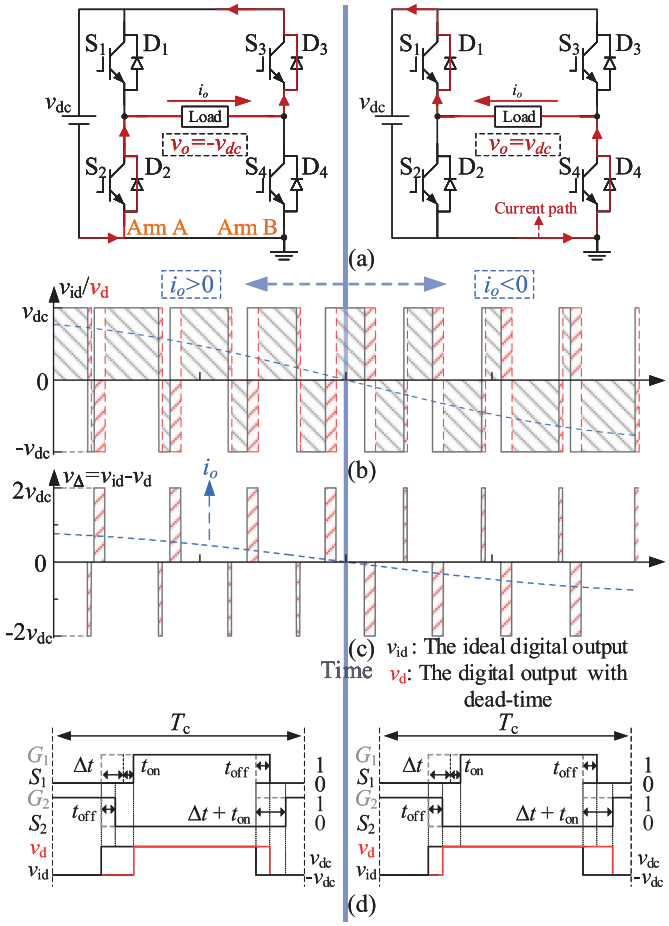

Fig. 3. Modulation process with dead time. (a) Current path and output voltage during dead time. (b) Output voltages before and after applying dead time. (c) Effect of dead time. (d) Detailed waveforms in one carrier period T_c.

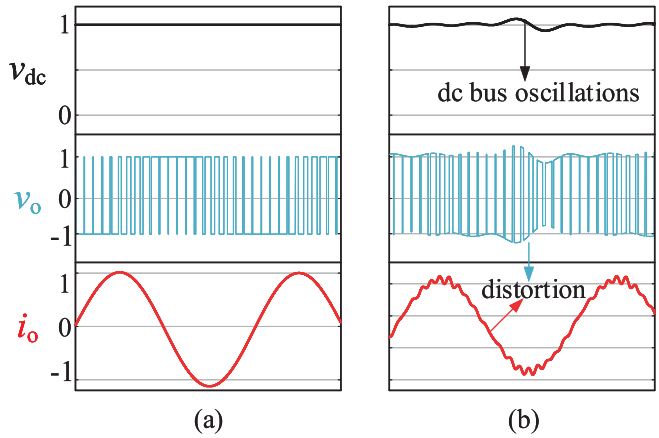

Fig. 4. Distortion caused by DC bus voltage ripple. (a) Converter system with ideal DC bus. (b) Converter system with DC bus oscillations.

The dead time is added just as the transistor is about to turn ON, causing a delay by Δt in the operation of this transistor, and after the turn OFF time t_{off}, the both switch devices on the same arm are in the OFF state. The polarity of the output voltage at this point will be determined by the current path through the antiparallel diodes, that is, the direction of the output current i_o.

Fig. 3(a) shows the current path and output voltage during the simultaneous OFF state, when the output current $i_o > 0$, the current passes through diodes D_2 and D_3, so the output voltage v_o is -v_{dc}; otherwise, when $i_o < 0$, the current passes through diodes D_1 and D_4 and the output voltage v_o is v_{dc}. This gives the variation pattern of the output voltage, and the detailed waveforms in one carrier period is shown in Fig. 3(d), where the gray dashed lines indicate the ideal switching signals G_1 and G_2 issued by the controller, and S_1 and S_2 indicate the actual states of the switching tubes. By analyzing Fig. 3(a) and (d), the influence of dead time and switching duration in the time domain can be obtained. When $i_o > 0$, the dead-time process will delay the rising and falling edges of the output voltage along $t_{\text{on}} + \Delta t$ (defined as t_d) and t_{off}, respectively, and the two times are opposite when $i_o < 0$.

The output voltages before and after applying the dead time are shown in Fig. 3(b), and the effect of introducing dead time on the output voltage in time domain is shown in Fig. 3(c), it can be seen that the dead time also brings a significant nonlinear effect to the system.

It is worth mentioning that if the switching tubes are defined as nonideal without considering the dead time, the simultaneous conduction will occur, therefore, in this article, the switching tubes are considered as ideal devices in the analysis without discussing the dead time. In addition, the turn ON and turn OFF signal of the actual device is a ramp, and this article uses area fitting to equate it to a straight up and down step signal for analysis, which does not affect the final results.

There is another factor that introduces a nonlinear effect to the system, the dc bus oscillations. When analyzing the harmonic spectrum of the inverter connected with the dc bus, it is usually assumed that the dc bus voltage contains only a pure dc component. For the dc bus with high-frequency voltage ripples, the harmonic components can be easily suppressed and this assumption is justified. However, for the dc bus voltage that experiences low-frequency oscillations, this assumption will not be valid. As shown in the comparison of Fig. 4(a) and (b), the low-frequency ripple in the dc bus voltage v_{dc} will introduce additional and nonnegligible harmonic components in the output voltage and current, especially in the low frequency. The effects of dc bus voltage oscillations will be described in detail later in Section IV.

III. Analytical Solution to the Harmonic Spectrum of VSI Output Voltage Under Ideal DC Bus

This section presents the well-established analytical solution for the output voltage harmonic spectrum of a single-phase VSI, and will use this solution to analyze the harmonic spectrum of the output voltage from the ideal model to the commonly used digital control model with disturbance in this and the next sections. The dc bus voltage in this section is assumed as ideally constant.

Fig. 5 shows the detailed digital PWM modulation process with dead time and dc bus oscillations effects. During each

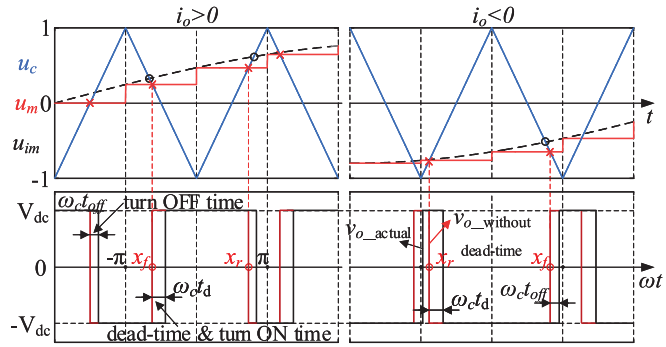

Fig. 5. Detailed modulation process with nonlinear factors during two carrier periods under different current polarity.

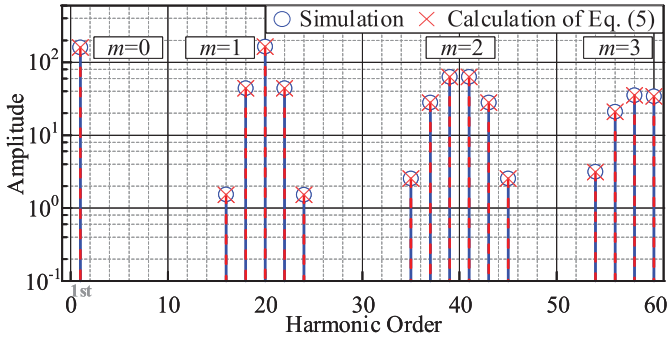

Fig. 6. Comparison of theoretical calculation and simulation results under natural sampling.

carrier period, the modulation waveform intersects the falling and rising edge of the triangle carrier with points X_f and X_r, respectively.

In the modulation process, the output voltage v_o changes with the comparative relationship of amplitude between the modulation waveform and the carrier, that is, the polarity of the output voltage changes at the intersection points if it is not affected by dead time.

Therefore, the expression of v_o is a time-varying function controlled by two variables related to the modulation waveform and carrier, respectively, thus a double Fourier series is introduced to express the output voltage as a weighted sum of harmonic components as follows:

$$v_o = \sum_{m=1}^{\infty} \sum_{n=\pm 1}^{\pm\infty} \begin{Bmatrix} A_{mn}\cos(mx+ny) \\ +B_{mn}\sin(mx+ny) \end{Bmatrix} \tag{1}$$

where m and n represent multiples of the frequency of carrier and modulation waveform, respectively. C_{mn} are the coefficients of the double Fourier series expansion, which also represent the amplitude and phase of each harmonic, and can be obtained by solving (2). The variables x and y are defined by (3), where ω_c and ω_m are the carrier and fundamental angular frequency, respectively, and the frequencies of harmonic components can be expressed as $m\omega_c + n\omega_m$.

$$\begin{aligned} C_{mn} &= A_{mn} + jB_{mn} \\ &= \frac{1}{2\pi^2}\int_{-\pi}^{\pi}\int_{-\pi}^{\pi} v_o \cdot e^{j(mx+ny)}dxdy \end{aligned} \tag{2}$$

$$x = \omega_c t, \quad y = \omega_m t \tag{3}$$

A. Ideal Harmonic Spectrum Under Natural Sampling

By making the equations of the ideal modulation waveform and carrier equal in time domain given in (A1) in Appendix, the coordinates of the intersection points X_f, X_r under natural sampling can be derived as

$$\begin{cases} X_r = \frac{\pi}{2}(1 + M\sin y) + 2p\pi \\ X_f = -\frac{\pi}{2}(1 + M\sin y) + 2p\pi \end{cases} \tag{4}$$

where $M = U_m/U_c$ is defined as the modulation ratio, and p is an arbitrary natural number.

Through the comparative relationship in PWM and the intersection (4), the time-domain expression of the output voltage without dead time can be obtained in (A2) in Appendix, which can be substituted into (2) to derive the coefficients A_{mn} and B_{mn} of the double Fourier series, and the specific solution procedure is provided in (A3) in Appendix, thereby the analytical harmonic spectrum of the ideal output voltage can be obtained by substituting into (1).

$$\begin{aligned} v_o^0(t) &= M\mathrm{V_{dc}}\sin(\omega_{\mathrm{m}}t) \\ &+ \sum_{m=1,3,5,\cdots}^{\infty} \frac{4\mathrm{V_{dc}}}{m\pi} J_0\left(\frac{mM\pi}{2}\right)\sin\frac{m\pi}{2}\cos(m\omega_c t) \\ &+ \sum_{m=1}^{\infty}\sum_{n=\pm1,\pm2,\cdots}^{\pm\infty} \left\{ \begin{matrix} \frac{4\mathrm{V_{dc}}}{m\pi} J_n\left(\frac{mM\pi}{2}\right)\sin\frac{(m+n)\pi}{2} \\ \cdot\cos\left(m\omega_{\mathrm{c}}t + n\omega_{\mathrm{m}}t - \frac{n\pi}{2}\right) \end{matrix} \right\} \end{aligned} \tag{5}$$

where $J_n(\frac{mM\pi}{2})$ is an nth-order Bessel function of the first kind, and the ideal dc bus voltage $v_{\mathrm{dc}} = V_{\mathrm{dc}}$.

A comparison of theoretical calculation of (5) and simulation results is shown in Fig. 6. The simulation results are obtained from FFT analysis of a VSI model built in MATLAB/Simulink, where the modulation ratio $M = 0.8$ and carrier ratio $N = \omega_c/\omega_m = 20$. Under natural sampling, the theoretical analysis results in (5) are in good agreement with the simulation results.

In addition, due to the large difference in amplitude between the output harmonic components, the vertical axis of the amplitude is changed to a logarithmic form in this article in order to better demonstrate the pattern of harmonic distribution.

It can be analyzed from the harmonic spectrum (5) and Fig. 6 that the ideal sinusoidal PWM (SPWM) output voltage contains a fundamental component that is proportional to M, the odd multiples of carrier harmonic components, the sideband harmonic components of the even -order $n = \pm(2, 4, 6\cdots)$ for the odd times of carrier frequencies and odd-order $n = \pm(1, 3, 5\cdots)$ for the even time of carrier frequencies, and no dc component.

The time-domain expression of the ideal output voltage and the harmonic spectrum of the output voltage in general form are provided in (A2)–(A4) in Appendix.

B. Ideal Harmonic Spectrum Under Digital Sampling

In the digital control system, the sampling points of the modulation waveform is fixed at the peaks $x_p = 2q\pi - \pi + \varphi_c$ and troughs $x_t = 2q\pi + \varphi_c$ of the carrier under the asymmetric regular sampling, where q is an arbitrary natural number and φ_c is the phase-shift angle of the carrier.

After sampling and passing through the zero-order holder (ZOH), the modulation waveform becomes a step wave, thus the phase angles of the staircase modulation waveform in each 2π carrier period can be expressed as continuous variables by the carrier ratio N and the carrier phase angles x_p, x_t at the sampling points as

$$\begin{cases} y_r = y - \frac{x}{N} + \frac{2q\pi+\varphi_c}{N} \\ y_f = y - \frac{x}{N} + \frac{2q\pi-\pi+\varphi_c}{N} \end{cases} \tag{6}$$

where y_r and y_f denote the phase angles of the modulation waveform when it intersects with the rising and falling edges of the carrier, respectively.

In this case, the intersection expression (4) derived in natural sampling will change as

$$\begin{cases} X_r = \frac{\pi}{2}(1 + M\sin y_r) + \varphi_c + 2p\pi \\ X_f = -\frac{\pi}{2}(1 + M\sin y_f) + \varphi_c + 2p\pi. \end{cases} \tag{7}$$

Same as the natural sampling, between two adjacent intersections, the output voltage is fixed as a positive or negative dc power supply, so the time-domain expression for the output voltage in Appendix (A2) still applies. However, the solution process for C_{mn} is altered due to the nonlinear effect introduced by sampling, and the coefficients C_{mn} can be calculated by (8), where the integral variables y_r and y_f have been replaced with y mathematically

$$\begin{aligned} C^0_{mn} = A^0_{mn} + jB^0_{mn} = & \frac{\mathrm{V_{dc}}}{2\pi^2} \cdot \\ & \left(-\int_{-\pi}^{\pi}\int_{-\pi}^{-\frac{\pi}{2}(1+M\sin y)+\varphi_c} e^{j(mx+n(y+\frac{x+\pi}{N}-\frac{\varphi_c}{N}))}dxdy \right. \\ & + \int_{-\pi}^{\pi}\int_{-\frac{\pi}{2}(1+M\sin y)+\varphi_c}^{0} e^{j(mx+n(y+\frac{x+\pi}{N}-\frac{\varphi_c}{N}))}dxdy \\ & + \int_{-\pi}^{\pi}\int_{0}^{\frac{\pi}{2}(1+M\sin y)+\varphi_c} e^{j(mx+n(y+\frac{x}{N}-\frac{\varphi_c}{N}))}dxdy \\ & \left. - \int_{-\pi}^{\pi}\int_{\frac{\pi}{2}(1+M\sin y)+\varphi_c}^{\pi} e^{j(mx+n(y+\frac{x}{N}-\frac{\varphi_c}{N}))}dxdy \right) \end{aligned} \tag{8}$$

Therefore, by solving (8), and then, applying it to (1), the output voltage harmonic spectrum of ideal digital SPWM that can be accurately analyzed and calculated is obtained as given in (9).

The comparison of theoretical calculation of (9) and simulation results is shown in Fig. 7, where the harmonic components with too small amplitude (less than 0.1 V) have been filtered, same as follows. Therefore, only the highlighted third harmonic in Fig. 7 is visible among the harmonic components introduced by digitization compared to Fig. 6.

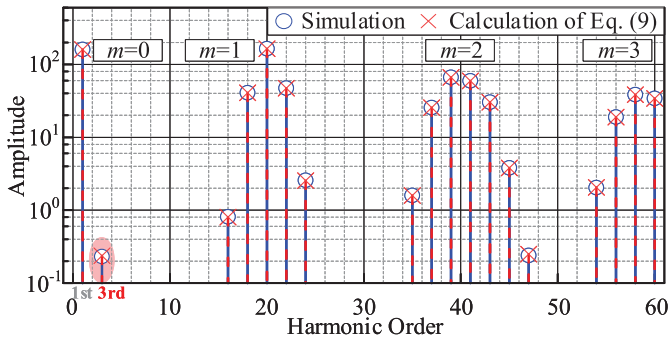

Fig. 7. Comparison of theoretical calculation and simulation results under digital sampling.

By comparing (5) and (9) as well as Figs. 6 and 7, it can be concluded that compared to the natural sampling situation, the nonlinear effect brought by fixed sampling points in the digital controller will introduce odd-order baseband harmonic components, change the phase of fundamental wave slightly, and have an impact on the amplitudes of the sideband harmonic components.

The impact of digitization on the system is related to the carrier ratio N. A larger carrier ratio means that the sampling frequency is higher and the digital sampling is closer to analog sampling, at which point, the impact of digitization on the system is reduced.

C. Harmonic Spectrum With Dead Time Under Digital Sampling

To avoid the short circuiting in the converter caused by the simultaneous conduction of the upper and lower transistors of the same arm, dead time Δt is introduced into the switching signals.

The dead time will delay the turn ON of the switch by Δt and will have a different effect on the output voltage depending on the output current directions, that is, the dead time will delay the rising and falling edges of the output voltage by t_d and t_{off} when the output current $i_o > 0$; and delay the rising and falling edges by t_{off} and t_d when $i_o < 0$. The specific analysis is given in Section II and Fig. 3.

After fully considering the error voltage caused by the dead time, a new time-domain expression of the output voltage with dead time can be obtained, which is provided in (A5) in Appendix. Since this expression is related to the current polarity, the calculation of double Fourier series coefficients in (2) needs to be changed into the form of half-periodic integral, and then, combined with (A5), as shown in Appendix (A6), it can be further derived as (10).

$$\begin{aligned} C^0_{mn} &= A^0_{mn} + jB^0_{mn} \\ &= j\frac{v_{dc}N}{\pi^2(mN+n)}e^{jm\varphi_c}. \end{aligned}$$

$$
\begin{aligned}
&\left(e^{j\left[(m+\frac{n}{N})\omega_c t_{off}-(m-\frac{n}{N})\frac{\pi}{2}\right]}\int_{-\pi+\varphi_i}^{\varphi_i} e^{jny}e^{-j\frac{\pi M}{2}(m+\frac{n}{N})\sin y}dy\right.\\
&-e^{j(m+\frac{n}{N})\left[\omega_c t_d+\frac{\pi}{2}\right]}\int_{-\pi+\varphi_i}^{\varphi_i} e^{jny}e^{j\frac{\pi M}{2}(m+\frac{n}{N})\sin y}dy\\
&+e^{j\left[(m+\frac{n}{N})\omega_c t_d-(m-\frac{n}{N})\frac{\pi}{2}\right]}\int_{\varphi_i}^{\pi+\varphi_i} e^{jny}e^{-j\frac{\pi M}{2}(m+\frac{n}{N})\sin y}dy\\
&\left.-e^{j(m+\frac{n}{N})\left[\omega_c t_{off}+\frac{\pi}{2}\right]}\int_{\varphi_i}^{\pi+\varphi_i} e^{jny}e^{j\frac{\pi M}{2}(m+\frac{n}{N})\sin y}dy\right) \quad (10)
\end{aligned}
$$

where $t_d = t_{\text{on}} + \Delta t$, represents the sum of the turn ON time and dead time, the coefficient of dc component C_{00} is zero, and φ_i is defined as the phase angle at which the output current lags the voltage, i.e., the phase angle at the current zero-crossing point.

Equation (10) is solved by the deformed form of the Jacobi–Anger expansion, and the calculable and analytical formula of the output voltage harmonic spectrum with dead time under digital sampling is given in (11), where the terms in the summations are added with variable k introduced by the Jacobi–Anger expansion.

The terms in (11) represent the baseband harmonic components, the carrier harmonic components, and sideband harmonic components in turn. Under the combined effects of dead time and digitization, the output voltage harmonic components only contain fundamental component, odd-order baseband, carrier harmonic components, as well as the sideband harmonic components in the vicinity of the parity-opposite carrier harmonic components, but do not contain dc component.

The comparison of simulation and calculation results with the combined effects of these two nonlinear factors is shown in

$$
\begin{aligned}
v_o^0 = &\sum_{n=1,3,5\ldots}^{+\infty}\frac{4NV_{dc}}{\pi n}J_n\left(\tfrac{nM\pi}{2N}\right)\left\{-\sin\left(\tfrac{n\pi}{2N}\right)\cos(n\omega_m t)+\cos\left(\tfrac{n\pi}{2N}\right)\sin(n\omega_m t)\right\}\\
&+\sum_{m=1,3,5\ldots}^{+\infty}\sum_{n=0,\pm2,\pm4\ldots}^{\pm\infty}\frac{4V_{dc}}{\pi\alpha}\sin\tfrac{m\pi}{2}J_n(\xi)\left\{\cos\left(\tfrac{n\pi}{2N}+m\varphi_c\right)\cos\left[(mN+n)\omega_m t\right]+\sin\left(\tfrac{n\pi}{2N}+m\varphi_c\right)\sin\left[(mN+n)\omega_m t\right]\right\}\\
&+\sum_{m=2,4,6\ldots}^{+\infty}\sum_{n=\pm1,\pm3\ldots}^{\pm\infty}\frac{4V_{dc}}{\pi\alpha}\cos\tfrac{m\pi}{2}J_n(\xi)\left\{-\sin\left(\tfrac{n\pi}{2N}+m\varphi_c\right)\cos\left[(mN+n)\omega_m t\right]+\cos\left(\tfrac{n\pi}{2N}+m\varphi_c\right)\sin\left[(mN+n)\omega_m t\right]\right\}\\
&\text{where } \alpha = m+\tfrac{n}{N},\ \xi = \tfrac{\pi M}{2}\left(m+\tfrac{n}{N}\right)
\end{aligned}
\quad (9)
$$

$$
\begin{aligned}
v_o^0 = &\operatorname{Re}\sum_{n=1,3,5\ldots}^{+\infty}\frac{4v_{dc}N}{\pi^2 n}e^{j\left(\frac{n\pi}{2N}+\frac{n\omega_c}{2N}(t_d+t_{off})\right)}e^{-jny}\cdot\\
&\left\{\begin{array}{l}2\sin\left(\frac{n\omega_c}{2N}(t_d-t_{off})\right)J_0\left(\frac{n\pi M}{2N}\right)\left(\frac{\sin n\varphi}{n}-j\frac{\cos n\varphi}{n}\right)+2\sin\left(\frac{n}{2N}\omega_c(t_d-t_{off})\right)\sum_{k=2,4,6\ldots}^{+\infty}J_k\left(\frac{n\pi M}{2N}\right)f_2(k,n)\\ +j\pi\cos\left(\frac{n\omega_c}{2N}(t_d-t_{off})\right)J_n\left(\frac{n\pi M}{2N}\right)\end{array}\right\}\\
&+\operatorname{Re}\sum_{m=1,3,5\ldots}^{+\infty}\sum_{n=0,\pm2,\pm4\ldots}^{\pm\infty}\frac{4V_{dc}}{\pi^2\alpha}\sin\left(\frac{m\pi}{2}\right)e^{j\left(m\varphi_k+\frac{n\pi}{2N}+\frac{\alpha\omega_c}{2}(t_d+t_{off})\right)}e^{-j(mx+ny)}\cdot\\
&\left\{2\sin\left(\frac{\alpha\omega_c}{2}(t_d-t_{off})\right)\sum_{k=1,3,5\ldots}^{+\infty}J_k(\xi)f_1(k,n)+\pi\cos\left(\frac{\alpha\omega_c}{2}(t_d-t_{off})\right)J_n(\xi)\right\}\\
&+\operatorname{Re}\sum_{m=2,4,6\ldots}^{+\infty}\sum_{n=\pm1,\pm3\ldots}^{\pm\infty}\frac{4V_{dc}}{\pi^2\alpha}\cos\left(\frac{m\pi}{2}\right)e^{j\left(m\varphi_k+\frac{n\pi}{2N}+\frac{\alpha\omega_c}{2}\omega_c(t_d+t_{off})\right)}e^{-j(mx+ny)}\cdot\\
&\left\{\begin{array}{l}2\sin\left(\frac{\alpha\omega_c}{2}(t_d-t_{off})\right)J_0(\xi)\left(\frac{\sin n\varphi}{n}-j\frac{\cos n\varphi}{n}\right)+2\sin\left(\frac{\alpha\omega_c}{2}(t_d-t_{off})\right)\sum_{k=2,4,6\ldots}^{+\infty}J_k(\xi)f_2(k,n)\\ +j\pi\cos\left(\frac{\alpha\omega_c}{2}(t_d-t_{off})\right)J_n(\xi)\end{array}\right\}\\
&\text{where } t_d = t_{on}+\Delta t,\\
&f_1(k,n)=\left(\frac{\cos(k+n)\varphi}{k+n}+\frac{\cos(k-n)\varphi}{k-n}\right)+j\left(\frac{\sin(k+n)\varphi}{k+n}-\frac{\sin(k-n)\varphi}{k-n}\right),\\
&f_2(k,n)=\left(\frac{\sin(k+n)\varphi}{k+n}+\frac{\sin(k-n)\varphi}{k-n}\right)-j\left(\frac{\cos(k+n)\varphi}{k+n}-\frac{\cos(k-n)\varphi}{k-n}\right)
\end{aligned}
\quad (11)
$$

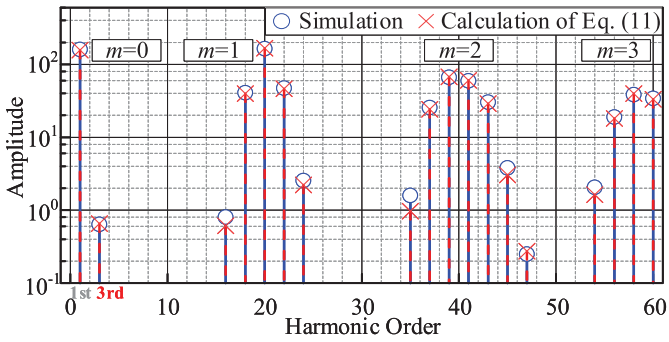

Fig. 8. Comparison of theoretical calculation and simulation results with effects of dead time and digitization.

Fig. 8, where it can be seen that the inclusion of dead time slightly affects the accuracy of several sideband harmonic components in the proposed analytical spectrum.

Compared with the ideal digital SPWM harmonic spectrum (9), the form of (11) becomes more complicated due to the dead time, but the composition of the output voltage harmonic components remains unchanged.

From (11), some conclusions can be drawn about the two nonlinear factors introduced so far: the amplitude of each harmonic component is linearly related to the dc bus voltage $v_{\rm dc}$, and is affected by the dead time Δt and carrier ratio N. And the baseband, sideband, and carrier harmonic components will be superimposed on each other, especially when the carrier ratio N is relatively small; however, it can be obtained from the computable (11) that the larger N will exacerbate the nonlinear effect of dead time, contrary to the effect of digitization.

The introduction of dead time does not change the harmonic distribution brought by digitization, but increases its amplitude, especially the baseband harmonic components in low frequency, such as the highlighted third harmonic component compared in Figs. 7 and 8.

IV. Analytical Solution to the Harmonic Spectrum of VSI Output Voltage Under Nonideal DC Bus

Since the low-frequency voltage ripple in the dc bus cannot be suppressed as easily as the high-frequency ripple, the effect of the nonideal dc bus voltage with considerable low-frequency harmonic components on the output is nonnegligible.

The frequencies of dc bus voltage harmonic components are defined in this article as multiples of the modulation waveform frequency for the sake of simplicity. The form of the dc bus voltage with ripples can be expressed as a pure dc component with the accumulation of harmonic components, as follows:

$$\begin{aligned} v_{\rm dc} &= v_{\rm dc}^0 + v_{\rm dc}^{h_1} + v_{\rm dc}^{h_2} + \cdots = v_{\rm dc}^0 + \sum_{h\in H} v_{\rm dc}^h \\ &= {\rm V_{dc}}\left[1 + \sum_{h\in H} \lambda_h \sin(h\omega_m t + \theta_h)\right] \end{aligned} \tag{12}$$

where $v_{\rm dc}^0$ is the pure dc component with value $V_{\rm dc}$, the product $\lambda_h \times V_{\rm dc}$ is the amplitude and θ_h is the phase-shift angle relative to the modulation waveform of the hth-order dc bus voltage harmonic. H is the set of harmonic orders, $h \in H$ and $H = \{h_1, h_2, h_3, \cdots\}$, where $h_1, h_2, h_3, \ldots$ are nonzero natural numbers.

The output voltage in this case can be seen as a superposition of the outputs from the different dc bus voltage harmonic components acting on the VSI system individually. Thus, the coefficients of the double Fourier series and the output voltage can be obtained as

$$C_{mn} = C_{mn}^0 + C_{mn}^{h_1} + C_{mn}^{h_2} + \cdots = C_{mn}^0 + \sum_{h\in H} C_{mn}^h \tag{13}$$

$$v_o = v_o^0 + v_o^{h_1} + v_o^{h_2} + \cdots = v_o^0 + \sum_{h\in H} v_o^h \tag{14}$$

where the coefficients C_{mn}^0 and output voltage v_o^0 under the ideal pure dc bus voltage are analyzed and shown in Sections III-A–C.

The case where the dc bus voltage is harmonic will be discussed next in this section to obtain the analytical harmonic spectrum of the total output voltage v_o in the VSI system.

In addition, the output voltage spectra considering dc bus oscillation under natural sampling has been analyzed previously in [36] and [37], it is less meaningful to repeat, so only the harmonic spectra under digital sampling is discussed in this article. However, the combined analysis of dc bus voltage oscillation with digital sampling and dead time is a challenge due to the high complexity of the derivation process and computation of the Fourier series, which is not mentioned in present article.

A. Harmonic Spectrum Without Dead Time Under Digital Sampling

It can be found from (12) that the dc bus harmonic components will introduce an additional function about y to the calculation of the double Fourier series coefficients C_{mn}^h, thus changing the integral form and bringing more harmonic components of the output voltage. When the dead time is not considered temporarily, the solution process for C_{mn}^h of the hth-order harmonic in the dc bus voltage referring (2) and (12) is shown as follows:

$$\begin{aligned} C_{mn}^h &= \frac{{\rm V_{dc}}\lambda_h}{2\pi^2} \\ &\cdot \left(-\int_{-\pi}^{\pi}\int_{-\pi}^{X_f} \sin(hy+\theta_h) e^{j(mx+n(y+\frac{x+\pi}{N}-\frac{\varphi_c}{N}))} dxdy \right. \\ &+ \int_{-\pi}^{\pi}\int_{X_f}^{0} \sin(hy+\theta_h) e^{j(mx+n(y+\frac{x+\pi}{N}-\frac{\varphi_c}{N}))} dxdy \\ &+ \int_{-\pi}^{\pi}\int_{0}^{X_r} \sin(hy+\theta_h) e^{j(mx+n(y+\frac{x}{N}-\frac{\varphi_c}{N}))} dxdy \\ &\left. - \int_{-\pi}^{\pi}\int_{X_r}^{\pi} \sin(hy+\theta_h) e^{j\left(mx+n\left(y+\frac{x}{N}-\frac{\varphi_c}{N}\right)\right)} dxdy \right) \end{aligned} \tag{15}$$

As can be seen in the previous analysis in this section, the dc component of the output voltage keeps zero when digitization and dead time are introduced, however, the dc bus voltage harmonic components will change this situation. When $m = n = 0$, the coefficient of the dc component of the output

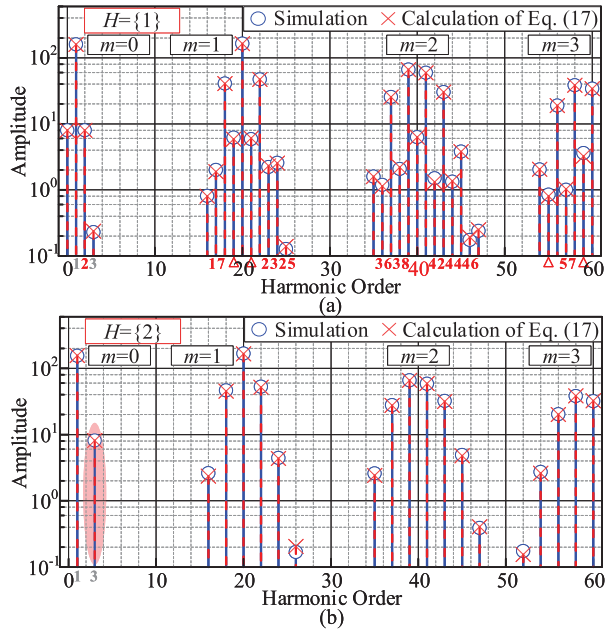

Fig. 9. Comparison of theoretical calculation and simulation results with DC bus oscillations in the digital system. (a) With first-order harmonic in DC bus voltage. (b) With second-order harmonic in the DC bus voltage.

voltage obtained by (15) can be expressed as (16). That is, the dc component will be introduced to the output voltage only when the dc bus voltage contains the first harmonic.

$$C_{00}^{h} = \frac{\mathrm{V_{dc}}\lambda_h M}{2\pi}\int_{-\pi}^{\pi}\sin y \sin(hy+\theta_h)dy = \frac{1}{2}\mathrm{V_{dc}}\lambda_h M\cos\theta_h\,|_{h=1} \tag{16}$$

Therefore, by solving (15) with a classification similar to (16) for each dc bus voltage harmonic, and then, applying to (13), the analytical harmonic spectrum of the total output voltage defined in (14) can be obtained in (17), where v_o^0 is the output voltage under the pure dc component of dc bus defined in (14), the detailed formula of v_o^0 is shown in (9) of Section III-B.

The comparison of theoretical calculation and simulation results with introducing a single odd- and even-order dc bus voltage harmonic, respectively, is shown in Fig. 9(a) and (b), and the simulation results are in agreement with (17).

The harmonic spectrum of v_o^h in (17) is kind of similar to the form of v_o^0, and the judgment condition of harmonic components is replaced by the parity of m and n to that of $m+h$ and $n+h$. However, with the addition of variable h, the distribution of output voltage harmonic components becomes complicated.

The theoretical analysis in (17) shows that the odd h will bring the even-order baseband and carrier harmonic components, as well as the sideband harmonic components in the vicinity of the parity-equal carrier groups to the output, which are exactly the opposite of parity of harmonic components brought by even-order harmonic components and pure dc component in the dc bus.

This conclusion can be verified from Fig. 9, where, for example, in Fig. 9(a), the first harmonic component in the dc bus introduces baseband and carrier harmonic components of frequencies $2\omega_m$ and $2\omega_c$ (orders 2 and 40), and sideband harmonic components of frequencies $\omega_c \pm \omega_m$ and $2\omega_c \pm 2\omega_m$(orders 19, 21 and 38, 42) and dc component (order 0); while these harmonic components are absent in Fig. 9(b), whose harmonic distribution is the same as that of Fig. 7 in Section III with the ideal dc bus voltage. However, the harmonic amplitudes in Fig. 9(b) are increased (compared with the highlighted third harmonic in Figs. 7 and 9), indicating that the second harmonic component in the dc bus repeatedly introduces the same output harmonic components as the pure dc bus voltage.

In particular, the dc component in the harmonic spectrum exists only when the dc bus contains the first-order harmonic component, and the fundamental component in it is only affected by the even-order harmonic components in the dc bus, as shown in Fig. 9 and (17), while $m=0$, $n=0$, and $n=1$.

B. Harmonic Spectrum With Dead Time Under Digital Sampling

With the aforementioned analysis, the three nonlinear factors discussed in this article will be combined in this subsection to obtain the harmonic spectrum of the total output voltage in the actual VSI system.

It can be concluded from the aforementioned analysis that the dead time changes the intersection of modulation waveform and triangular carrier in the digital SPWM process, and

$$\begin{aligned}
v_o = {} & v_o^0 + \frac{1}{2}V_{dc}\lambda_{\mathrm{h}} M\cos(\theta_h)\Big|_{h=1} \\
& + \mathrm{Re}\sum_{n=1}^{+\infty}\left(\sum_{h\in H}^{+\infty}\left\{\frac{2V_{dc}\lambda_{\mathrm{h}}N}{\pi n}\left[J_{(n+h)}\left(\frac{n\pi M}{2N}\right)e^{j\left(\frac{n\pi}{2N}+\theta_h\right)} - J_{(n-h)}\left(\frac{n\pi M}{2N}\right)e^{j\left(\frac{n\pi}{2N}-\theta_h\right)}\right]\Big|_{n+h=1,3,5\ldots}\right\}e^{-jny}\right) \\
& + \mathrm{Re}\sum_{m=1,3,5\ldots}^{+\infty}\sum_{n=\pm1}^{\pm\infty}\left(\sum_{h\in H}\left\{j\frac{2V_{dc}\lambda_{\mathrm{h}}}{\pi\alpha}\sin\left(\frac{n\pi}{2N}\right)e^{j\left(\frac{n\pi}{2N}-\frac{n\varphi_c}{N}\right)}\left(e^{-j\theta_h}\Big|_{n=h} - e^{j\theta_h}\Big|_{n=-h}\right)\right\}e^{-j(mx+ny)}\right) \\
& + \mathrm{Re}\sum_{m=1}^{+\infty}\sum_{n=0,\pm1,\pm2\ldots}^{\pm\infty}\left(\sum_{h\in H}\left\{j\frac{2V_{dc}\lambda_h}{\pi\alpha}\left(\begin{array}{l}+\sin\left(\frac{m+n-h}{2}\pi\right)J_{(n-h)}(\xi)e^{j\left(m\varphi_c+\frac{n\pi}{2N}-\theta_h+\frac{n-h}{2}\pi\right)} \\ -\sin\left(\frac{m+n+h}{2}\pi\right)J_{(n+h)}(\xi)e^{j\left(m\varphi_c+\frac{n\pi}{2N}+\theta_h+\frac{n+h}{2}\pi\right)}\end{array}\right)\Big|_{m+n+h=1,3,5\ldots}\right\}e^{-j(mx+ny)}\right)
\end{aligned} \tag{17}$$

therefore, changes the limits of integration in the calculation of the double Fourier series coefficients, as can be seen in (10) and (A3), while dc bus harmonic components are related to the fundamental frequency and introduce a new integral function in that calculation, as shown in (15). Thus, when combining these two nonlinear factors and considering the effect of digitization, both the limits of integration and the integral function of the coefficient calculation (8) in Section III-B will be changed.

With the combination of dead time and dc bus harmonic components in the digital system, the coefficients of the double Fourier series for output voltage harmonic spectrum can be calculated by

$$\begin{aligned} C_{mn}^{h} &= j\tfrac{\mathrm{V_{dc}}\lambda_h}{2\pi^2\alpha}e^{-j\frac{n}{N}\varphi_c}(e^{j\pi m}-1) \\ &\cdot(e^{-j\pi m}+e^{j\frac{n}{N}\pi})\int_{-\pi+\varphi_i}^{\pi+\varphi_i}\sin(hy+\theta_h)e^{jny}dy \\ &+j\tfrac{\mathrm{V_{dc}}\lambda_h}{\pi^2\alpha}e^{j(m\varphi_c+\frac{n\pi}{2N})} \\ &\left\{\cdot\int_{-\pi+\varphi_i}^{\varphi_i}\cdot\begin{pmatrix}\sin(hy+\theta_h)e^{jny}\\ e^{-j\frac{\pi m}{2}}e^{-j\xi\sin y}e^{j\alpha\omega_c t_{off}}\\ -e^{j\frac{\pi m}{2}}e^{j\xi\sin y}e^{j\alpha\omega_c t_d}\end{pmatrix}dy\right. \\ &\left.+\int_{\varphi_i}^{\pi+\varphi_i}\cdot\begin{pmatrix}\sin(hy+\theta_h)e^{jny}\\ e^{-j\frac{\pi m}{2}}e^{-j\xi\sin y}e^{j\alpha\omega_c t_d}\\ -e^{j\frac{\pi m}{2}}e^{j\xi\sin y}e^{j\alpha\omega_c t_{off}}\end{pmatrix}dy\right\}. \end{aligned} \tag{18}$$

Due to space issues, this equation has been simplified when m and n are not all zero at the same time.

In particular, when applying $m=n=0$, the coefficients of the dc component in the output voltage harmonic spectrum can be obtained by the following equation:

$$C_{00}^{h}=\frac{\mathrm{V_{dc}}\lambda_h}{\pi^2}\cdot\left\{\begin{array}{l}\pi\mathrm{M}\int_{-\pi+\varphi_i}^{\pi+\varphi_i}\sin\mathrm{y}\sin(\mathrm{hy}+\theta_\mathrm{h})\mathrm{dy}\\ +\omega_c(t_d-t_{off})\\ \cdot\left(\begin{array}{l}\int_{-\pi+\varphi_i}^{\varphi_i}\sin(hy+\theta_h)dy\\ -\int_{\varphi_i}^{\pi+\varphi_i}\sin(hy+\theta_h)dy\end{array}\right)\end{array}\right\}. \tag{19}$$

Then, by solving (18) and (19) and applying to (13), the analytical harmonic spectrum of the total output voltage in the actual VSI system with multiple nonlinear factors can be obtained as (20), where v_o^0 is the output voltage under the pure dc component of the dc bus voltage.

The different output voltage harmonic spectra when the dc bus voltage contains odd- and even-order harmonic components, i.e., $H=\{1\}$ and $H=\{2\}$ obtained from the theoretical calculation in (20) and simulation results are presented in Fig. 10(a) and (b), respectively. Besides, the harmonic spectrum of the VSI output voltage under the ideal pure dc bus voltage has been presented in Fig. 8.

By comparing Figs. 8 with 10, the effect of dc bus harmonic components can be clearly identified. The spectrum in Fig. 10(a) contains the even-order baseband (second) and carrier harmonic

$$\begin{aligned} v_o &= v_o^0+\left.\frac{1}{2}V_{dc}\lambda_h M\cos(\theta_h)\right|_{h=1}-\sum_{\substack{h=1,3,5\ldots\\ h\in H}}\frac{2V_{dc}\lambda_\mathrm{h}\omega_c}{h\pi^2}(t_d-t_{off})\cos(\theta_h+\varphi_i) \\ &+\mathrm{Re}\left.\left\{\begin{array}{l}\sum_{n=1}^{+\infty}\sum_{h\in H}\frac{2V_{dc}\lambda_h N}{n\pi^2}e^{j(\frac{n\pi}{2N}+\frac{n\omega_c}{2N}(t_d+t_{off}))}e^{-jny}\cdot\\ \pi\cos(\frac{\mathrm{n}\omega_c}{2\mathrm{N}}(\mathrm{t_d}-\mathrm{t_{off}}))(\mathrm{J_{n+h}}(\frac{\mathrm{n}\pi\mathrm{M}}{2\mathrm{N}})\mathrm{e}^{\mathrm{j}\theta_\mathrm{h}}-\mathrm{J_{n-h}}(\frac{\mathrm{n}\pi\mathrm{M}}{2\mathrm{N}})\mathrm{e}^{-\mathrm{j}\theta_\mathrm{h}})-\mathrm{j}\sin(\frac{\mathrm{n}\omega_c}{2\mathrm{N}}(\mathrm{t_d}-\mathrm{t_{off}}))\mathrm{J_0}(\frac{\mathrm{n}\pi\mathrm{M}}{2\mathrm{N}})\mathrm{f_3(n,h,0)}\\ -2j\sin(\frac{n\omega_c}{2N}(t_d-t_{off}))\sum_{k=2,4,6\ldots}^{+\infty}J_k(\frac{n\pi M}{2N})f_3(n,h,k)\end{array}\right\}\right|_{n+h=1,3,5\ldots} \\ &+\mathrm{Re}\sum_{m=1,3,5\ldots}^{+\infty}\sum_{n=\pm1}^{\pm\infty}\sum_{h\in H}j\frac{2V_{dc}\lambda_\mathrm{h}}{\pi\alpha}\sin\left(\frac{n\pi}{2N}\right)e^{j\left(\frac{n\pi}{2N}-\frac{n\varphi_c}{N}\right)}(e^{-j\theta_h}\big|_{n=h}-e^{j\theta_h}\big|_{n=-h})e^{-j(mx+ny)} \\ &+\mathrm{Re}\left.\left\{\begin{array}{l}\sum_{m=1,3,5\ldots}^{+\infty}\sum_{n=0,\pm1\ldots}^{\pm\infty}\sum_{h\in H}j\frac{2V_{dc}\lambda_\mathrm{h}}{\pi^2\alpha}\sin(\frac{m\pi}{2})e^{j(m\varphi_c+\frac{n\pi}{2N}+\frac{\alpha\omega_c}{2}(t_d+t_{off}))}e^{-j(mx+ny)}\cdot\\ \pi\cos(\frac{\alpha\omega_c}{2}(t_d-t_{off}))(J_{n-h}(\xi)e^{-j\theta_h}-J_{n+h}(\xi)e^{j\theta_h})+2\sin(\frac{\alpha\omega_c}{2}(t_d-t_{off}))\sum_{k=1,3,5\ldots}^{+\infty}J_k(\xi)f_4(n,h,k)\end{array}\right\}\right|_{n+h=0,2,4\ldots} \\ &+\mathrm{Re}\left.\left\{\begin{array}{l}\sum_{m=2,4,6\ldots}^{+\infty}\sum_{n=0,\pm1\ldots}^{\pm\infty}\sum_{h\in H}\frac{2V_{dc}\lambda_\mathrm{h}}{\pi^2\alpha}\cos(\frac{m\pi}{2})e^{j(m\varphi_c+\frac{n\pi}{2N}+\frac{\alpha\omega_c}{2}(t_d+t_{off}))}e^{-j(mx+ny)}\cdot\\ \pi\cos(\frac{\alpha\omega_c}{2}(\mathrm{t_d}-\mathrm{t_{off}}))(\mathrm{J_{n+h}}(\xi)\mathrm{e}^{\mathrm{j}\theta_\mathrm{h}}-\mathrm{J_{n-h}}(\xi)\mathrm{e}^{-\mathrm{j}\theta_\mathrm{h}})-\mathrm{j}\sin(\frac{\alpha\omega_c}{2}(\mathrm{t_d}-\mathrm{t_{off}}))\mathrm{J_0}(\xi)\mathrm{f_3(n,h,0)}\\ -2j\sin(\frac{\alpha\omega_c}{2}(t_d-t_{off}))\sum_{k=2,4,6\ldots}^{+\infty}J_k(\xi)f_3(n,h,k)\end{array}\right\}\right|_{n+h=1,3,5\ldots} \end{aligned}$$

where

$$\begin{aligned} f_3(n,h,k) &= \frac{e^{j((n+h+k)\varphi_i+\theta_h-\frac{\pi}{2})}}{n+h+k}-\frac{e^{j((n+h-k)\varphi_i+\theta_h+\frac{\pi}{2})}}{n+h-k}-\frac{e^{j((n-h+k)\varphi_i-\theta_h-\frac{\pi}{2})}}{n-h+k}+\frac{e^{j((n-h-k)\varphi_i-\theta_h+\frac{\pi}{2})}}{n-h-k}, \\ f_4(n,h,k) &= -\frac{e^{j((n+h+k)\varphi_i+\theta_h)}}{n+h+k}+\frac{e^{j((n+h-k)\varphi_i+\theta_h)}}{n+h-k}+\frac{e^{j((n-h+k)\varphi_i-\theta_h)}}{n-h+k}-\frac{e^{j((n-h-k)\varphi_i-\theta_h)}}{n-h-k} \end{aligned} \tag{20}$$

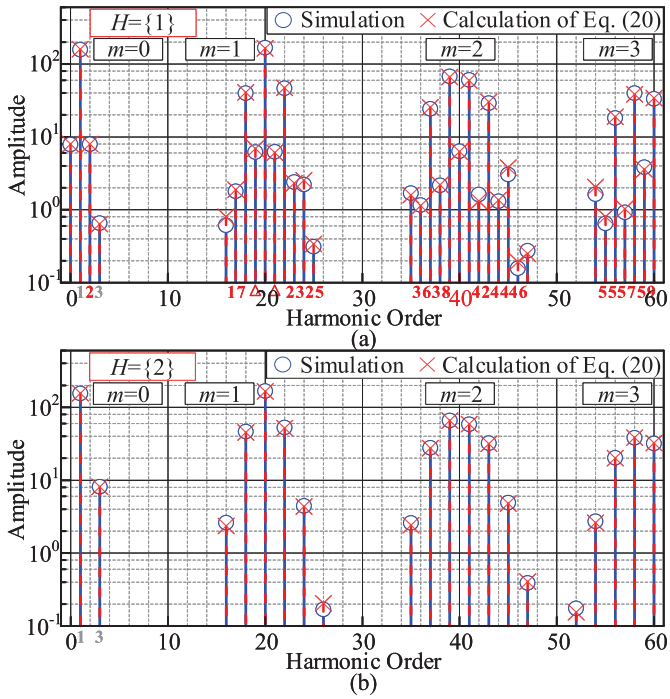

Fig. 10. Comparison of theoretical calculation and simulation results with dead time and DC bus oscillations in digital system. (a) With first-order harmonic in the DC bus voltage. (b) With second-order harmonic in DC bus voltage.

TABLE II
EXACT AMPLITUDES OF TYPICAL HARMONIC COMPONENTS

			Harmonic Amplitudes (V)		
Harmonic Order	m	n	H=∅	H=1	H=2
0	0	0	0	8	0
1	0	1	159.9	159.9	156.1
2	0	2	0	7.9	0
3	0	3	0.2	0.2	8.08
18	1	-2	40.6	40.6	46.4
19	1	-1	0	6.9	0
20	1	0	163.6	163.6	165.8
38	2	-2	0	2.2	0
39	2	-1	66.5	66.5	65.6
40	2	0	0	6.3	0
Harmonic distribution			-	Changed	Unchanged
Original Amplitudes			-	Unchanged	Changed

components (40th), and both the odd- and even-order sidebands appear in the even carrier group (m=2). Especially, the dc component is introduced and the amplitude of each original harmonic component in Fig. 8 is not affected by the odd-order dc bus harmonic components. Meanwhile, the spectrum in Fig. 10(b) does not introduce new harmonic components compared to Fig. 8, but the amplitude of the original harmonic components is affect.

In order to have a better analysis of the effects of different dc bus harmonic components, the exact amplitudes of some typical harmonic components are listed in Table II, where the data for $H = \varnothing$ are derived from Fig. 8, and also the data in the last two rows of the table are used for comparison.

Up to this point, the effect of dc bus voltage harmonic components on output harmonic components can be summarized from the analysis of the aforementioned two subsections.

The harmonic distribution of the actual output voltage can be obtained from the spectrum (20). The harmonic components of the total output voltage can be divided into two parts, one of which is the output voltage v_o^0 under the effect of pure dc component in dc bus voltage, and this part has been already analyzed in detail in Section III-C and (11).

The other part is the output harmonic components under the effect of the dc bus voltage harmonic components, and the conditions for judging the position of output harmonic components are changed to be related to the order h of dc bus harmonic components, which are the same as the system without dead time shown in (17). The conditions for determining the existence of the baseband, carrier, and sideband harmonic components in output voltage have changed from n, m, and $m+n$ being an odd to $n+h$, $m+h$, and $m+n+h$ being odd, respectively .

That is, the harmonic distribution of the output voltage v_o^h brought by an even-order dc bus harmonic is identical with the initial output voltage v_o^0, this means that the even hth-order dc bus voltage harmonic components will not introduce the dc component and harmonic components at new positions in the output voltage, but will change the amplitude and phase of the original harmonic components [see an example of the first and third harmonic components and the comparison of Figs. 8 and 10(b)]. In contrast, an odd-order dc bus harmonic does not affect the original harmonic components, but introduces new output harmonic components with a different distribution [see an example of the 2nd and 19th harmonic components and the comparison of Figs. 8 and 10(a)], and in particular, the odd-order dc bus harmonic components introduce a dc component in output voltage.

V. CONCLUSION ABOUT THE EFFECTS OF NONLINEAR FACTORS

Based on the aforementioned theoretical analysis, when the digital control system is affected by the nonlinear factors of dead time and dc bus voltage harmonic components, the harmonic spectrum of output voltage will not only contain the odd-order baseband and carrier harmonic components and the sideband harmonic components in the vicinity of the parity-opposite carrier groups, but also contain the additional output harmonic components of different positions and dc components when the dc bus voltage contains odd-order harmonic components; where the parities of the variables m and n of these additional harmonic components are exactly opposite to the corresponding output harmonic components introduced by the pure dc component of the dc bus. Furthermore, different kinds of harmonic components will be superimposed on each other.

With the proposed harmonic spectra and the aforementioned analysis, the effect of three different nonlinear factors on the output voltage can be concluded as follows.

1) *The effects of digitization:* Compared to the analog system, digital sampling causes a delay to the modulation waveform. Therefore, digitization introduces odd-order baseband harmonic components, and changes the amplitude and phase of sideband harmonic components, but it does not change those of fundamental and carrier harmonic components. This conclusion can be verified by comparing the harmonic spectra (5) with (9).
   Moreover, since the carrier ratio represents the sampling rate, the smaller the carrier ratio N, the more pronounced the effect of digitization on the system.
2) *The effects of dead time:* Under the same conditions, the introduction of dead time in the digital system will not change the harmonic distribution of output voltage, but will affect the original harmonic components. This means that the dead time does not introduce additional harmonic components, but changes the amplitude and phase of each harmonic, especially the baseband and sideband harmonic components. The extent of effect of the dead time on the system is related to the size of Δt.
   Under the same dc bus conditions change from Fig. 8 [see (11)] to Fig. 10 [see (20)] is consistent with the change from Fig. 7 [see (9)] to Fig. 9 [see (17)], and the harmonic distribution in Fig. 10 does not change with respect to Fig. 9, but the harmonic amplitudes change (such as 3rd and 25th), as well as the comparison between Figs. 7 and 8. These comparisons prove the conclusion again that the introduction of dead time does not change the harmonic distribution regardless of the presence of dc bus harmonic components but increases the harmonic amplitudes.
3) *The effects of DC bus oscillations:* From the form of (20), the effects caused by the nonlinear factor of dc bus voltage harmonic components in the digital system can be divided into two types by the parity of the harmonic components in the dc bus voltage: the even-order dc bus voltage harmonic components will bring the same output harmonic components as the original harmonic distribution, thus the amplitude and phase of each original harmonic are changed; and the dc component and additional harmonic components of the output voltage that do not overlap with the original harmonic distribution are introduced when the dc bus voltage contains odd-order harmonic components. In other words, the even-order dc bus harmonic components will repeatedly introduce the output harmonic components with frequencies of $\omega_{\rm m}, 3\omega_{\rm m}, \omega_{\rm c}, 3\omega_{\rm c}, \omega_{\rm c} \pm 2\omega_{\rm m}$, $2\omega_{\rm c} \pm \omega_{\rm m}$, and so on, while the odd dc-order dc bus harmonic components will introduce different output harmonic components with frequencies of $0, 2\omega_{\rm m}, 4\omega_{\rm m}, 2\omega_{\rm c}$, $4\omega_{\rm c}, \omega_{\rm c} \pm \omega_{\rm m}, 2\omega_{\rm c} \pm 2\omega_{\rm m}$, and so on.
   It can be obtained from (20) that the effects of dc bus oscillations are associated with the size of dead time, the total amount of harmonic components in the dc bus voltage, and the coefficient of amplitude λ_h, and are proportional to λ_h . The nonideal dc bus voltage with multiple harmonic components can introduce extra output harmonic components while also altering the original harmonic components, causing a significant impact on the output harmonic spectrum of the converter system.
4) *The combined effects caused by nonlinear factors:* The effects of nonlinear factors of digitization, dead time, and nonideal dc bus voltage will superimpose on each other, strengthening or weakening the impact of one factor or the other.
   With the computable spectrum (20) proposed in this article, the effects of the combined introduction of these nonlinear factors are quantified and the accurate conclusions are given for the first time.
   a) *The dc component in output voltage:* The combined effect of nonlinear factors on the dc component of the output voltage can be obtained from (19). The upper term is nonzero only when h=1, meaning that the first-order dc bus harmonic will have an additional effect on the dc component of the output voltage. This term is free of dead time effect and corresponds to (16).
      The lower part represents the superimposed effect of dead time and dc bus harmonic components, where every odd-order dc bus harmonic component (no longer only the 1^{st}) will affect the dc component of the output under the combined influence of dead time. The aforementioned analysis can be corresponded to the first term in (20), and is rewritten as follows.

$$v_{o0} = \frac{1}{2} V_{\rm dc} \lambda_h M \cos(\theta_h)\Big|_{h=1} - \sum_{\substack{h=1,3,5\ldots \\ h\in H}} \frac{2V_{dc}\lambda_{\rm h}\omega_c}{h\pi^2}\left(t_d - t_{\rm off}\right)\cos(\theta_h + \varphi_i). \tag{21}$$

      It can be concluded that with the increasing of dead time Δt or the amplitudes of the odd-order dc bus harmonic components, the dc component in output voltage will be affected more drastically. And in addition, digitization does not affect the dc component in output voltage.
   b) *The harmonic components in output voltage:* The harmonic components of the output voltage can be seen as a synthesis of the harmonic components introduced by these three nonlinear factors. The change of these factors will affect the harmonic amplitude, it is apparent form (20) that the larger dead time and higher content of dc bus harmonic components will increase the output harmonic components and THD.

However, since in the modern digital control system, the amplitude of output harmonic components introduced by those factors are all related to the carrier ratio N, the effect of the carrier ratio, i.e., the sampling rate, on the system needs to be studied further.

Take the third harmonic component as an example, the expressions v_{i3}, v_{d3}, and v_{r3} for the third harmonic component introduced by the digitization, dead time, and dc bus harmonic

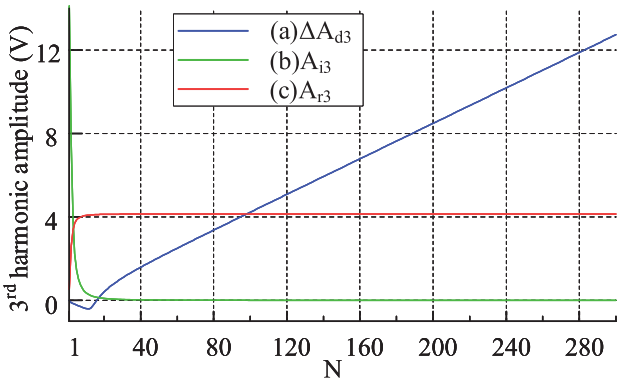

Fig. 11. Effect of the sampling rate on amplitudes of output harmonic introduced by nonlinear factors. (a) Dead time. (b) Digitization. (c) DC bus ripple.

components, respectively, are shown as follows:

$$v_{i3} = \mathrm{Re}\frac{4NV_{\mathrm{dc}}}{3\pi} J_3\left(\frac{3M\pi}{2N}\right) e^{j\left(\frac{3\pi}{2N}+\frac{\pi}{2}\right)} e^{-j3y} \tag{22}$$

$$\begin{aligned} v_{d3} + v_{i3} = \mathrm{Re}&\frac{4\mathrm{V}_{dc}N}{3\pi^2} e^{j\left(\frac{3\pi}{2N}+\frac{n\omega_c}{2N}(t_d+t_{\mathrm{off}})\right)} e^{-j3y} \\ \cdot&\left\{ \begin{array}{l} 2\sin\left(\frac{3\omega_c}{2N}\left(t_d - t_{\mathrm{off}}\right)\right) \\ \cdot\left(\begin{array}{l} J_0\left(\frac{3\pi M}{2N}\right)\left(\frac{\sin 3\varphi}{3} - j\frac{\cos 3\varphi}{3}\right) \\ +\sum\limits_{k=2,4,6\ldots}^{+\infty} J_k\left(\frac{3\pi M}{2N}\right) f_2(k,3) \end{array} \right) \\ +j\pi\cos\left(\frac{3\omega_c}{2N}\left(t_d - t_{\mathrm{off}}\right)\right) J_n\left(\frac{3\pi M}{2N}\right) \end{array} \right\} \end{aligned} \tag{23}$$

$$\begin{aligned} v_{r3} = \mathrm{Re}&\sum_{\substack{h=2,4,6\ldots \\ h\in H}} \frac{2V_{dc}\lambda_h N}{3\pi^2} e^{j\left(\frac{3\pi}{2N}+\frac{3\omega_c}{2N}(t_d+t_{off})\right)} e^{-j3y} \\ \cdot&\left\{ \begin{array}{l} \pi\cos\left(\frac{3\omega_c}{2N}\left(\mathrm{t_d} - \mathrm{t_{off}}\right)\right)\left(\begin{array}{l} J_{3+\mathrm{h}}\left(\frac{3\pi M}{2N}\right) e^{j\theta_h} \\ -J_{3-\mathrm{h}}\left(\frac{3\pi M}{2N}\right) e^{-j\theta_h} \end{array} \right) \\ -j\sin\left(\frac{3\omega_c}{2N}\left(t_d - t_{\mathrm{off}}\right)\right) \\ \cdot\left(\begin{array}{l} J_0\left(\frac{3\pi M}{2N}\right) f_3(3,h,0) \\ +2\sum\limits_{k=2,4,6\ldots}^{+\infty} J_k\left(\frac{3\pi M}{2N}\right) f_3(3,h,k) \end{array} \right) \end{array} \right\}. \end{aligned} \tag{24}$$

Keeping other conditions fixed, and with carrier ratio N as the variable, a plot of the function between the amplitude of third harmonic and N can be obtained to study the effect of the sampling rate on the output harmonic components, as shown in Fig. 11.

As the sampling rate, i.e., the carrier ratio N, increases, the amplitude of output harmonic introduced by the dead time will increase significantly, while the harmonic introduced by digitization will tend to zero. Meanwhile, the sampling rate does not affect the harmonic components introduced by the dc bus voltage oscillation. These results are consistent with the expected analysis.

The superposition of the three nonlinear factors will make the output harmonic components increase and be irregularly distributed, making it difficult to accurately calculate and eliminate the harmonic components of the output voltage.

However, the analytical and computable harmonic spectrum proposed in this article can accurately calculate the harmonic distribution as well as the amplitude and phase of each harmonic component. Based on this, the proposed work can provide a theoretical basis for system parameter design and high-precision harmonic compensation or elimination, such as calculating the optimal dead time and sampling rate, designing an efficient filter and controller based on the harmonic distribution, or using inverse compensation for precise elimination of specific harmonic components. An example of the application for calculation of optimal dead time is shown in Appendix G.

Importantly, the proposed work based on the bipolar modulation strategy is highly scalable and can be easily extended to harmonic analysis for various situations such as cascade, parallel structures, unipolar frequency doubling modulation strategy, and three-phase systems in the similar manner. And for example, the results extended to the unipolar modulation strategy are shown in Appendix H.

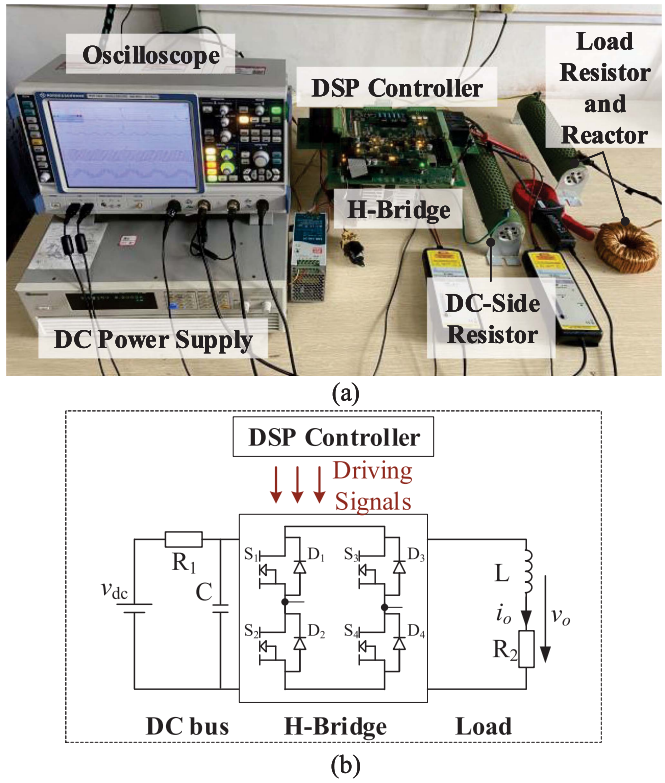

Fig. 12. Experimental prototype of a single-phase H-bridge VSI. (a) Experimental platform. (b) Circuit diagram.

VI. Experimental Results

To verify the correctness of the aforementioned theoretical analysis, a single-phase H-bridge VSI prototype, presented in Fig. 12(a), was developed. The transistors in HB are from the SIC module (CCS050M12CM2) produced by Wolfspeed (CREE), and the controller is based on DSP (TMS320F28377D). The dc bus voltage is generated by a programmable dc power supply (Chroma 62150H-600S). Fig. 12(b) shows the experimental circuit diagram, and the main parameters are listed in Table III.

Due to the limitations of the experimental conditions, the SiC module was chosen for the switching tubes, however, our

TABLE III
MAIN EXPERIMENTAL PARAMETERS

Symbol	Parameters	Value
V_{dc}	Ideal dc bus voltage	200 V
f_m	Modulation frequency	50 Hz
f_c	Carrier frequency	1,2,10 kHz
M	Modulation ratio	0.8
N	Carrier ratio	20,40,200
R_1	DC-side resistance	4 Ω
C	DC bus capacitor	550 μF
L	Load inductance	4 mH
R_2	Resistive load	8 Ω

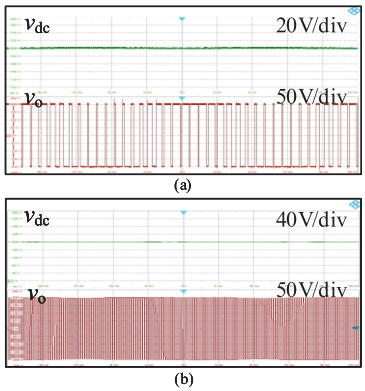

Fig. 13. Experimental waveforms without dead time and DC bus oscillations. (a) Carrier ratio $N = 20$. (b) Carrier ratio $N = 200$.

proposed results are device independent, and therefore, do not affect the accuracy of the experimental results. And the dc bus voltage cannot be controlled to follow an arbitrary reference, so this article amplifies the existing dc bus ripple by connecting a resistor in series on the dc side, and then, uses the FFT technique to obtain the harmonic components of the dc bus voltage. These harmonic components are substituted into the formulas of output harmonic spectra proposed previously, so as to compare with the experiment data of the output voltage.

For further analysis, the collected output voltage experimental data are imported into MATLAB, and the FFT technique is applied so that the amplitude of each harmonic can be accurately compared with the theoretical calculation.

A. Experimental Results With Effects of Digitization

Figs. 13 and 14 show the results obtained from the open-circuit experiments under different carrier ratios, i.e., they are free from dead time and dc bus voltage oscillations. The dc bus voltage v_{dc} and output voltage v_o at carrier ratios N=20 and 200 are presented in Fig. 13(a) and (b), and the comparisons of amplitude and phase of each harmonic component in experiment and theory calculation by (9) can be seen in Fig. 14(a) and (b).

From Fig. 14, it can be seen that the proposed analytical harmonic spectrum (9) is consistent with the open-circuit experiments under different carrier ratios, and the harmonic distributions are in agreement with previous analysis.

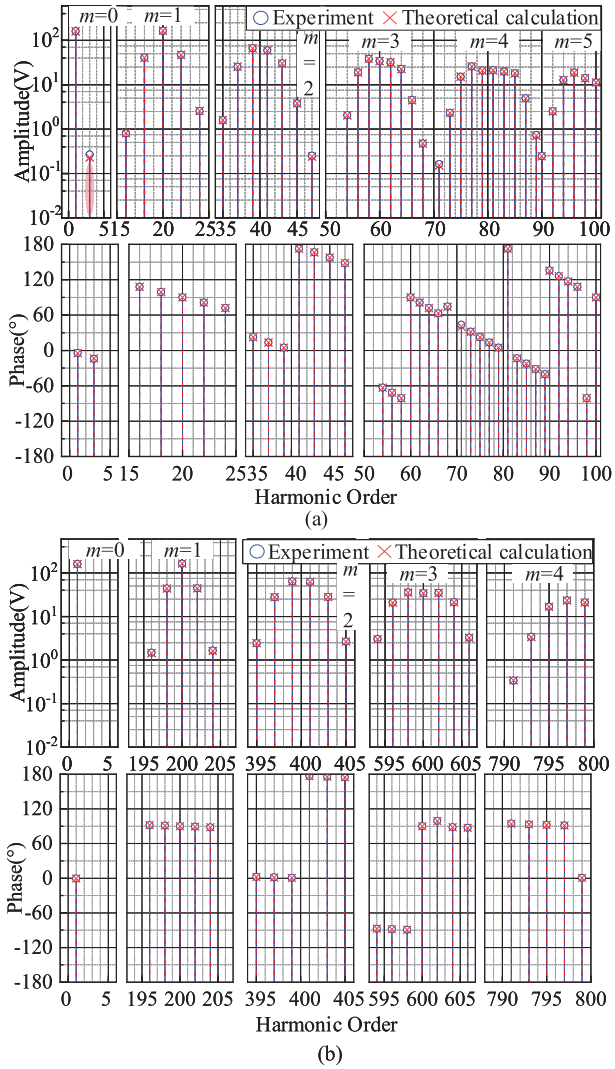

Fig. 14. Comparison of experimental and calculation results of output harmonic components without dead time and DC bus oscillations. (a) Carrier ratio $N = 20$. (b) Carrier ratio $N = 200$.

Furthermore, in the previous analysis, since the carrier ratio represents the sampling rate, a smaller N will increase the harmonic amplitude, which means that a small N will increase the impact of digitalization. This phenomenon can be verified by comparing the harmonic amplitudes or THD in Fig. 14(a) and (b), such as the highlighted third harmonic.

B. Experimental Results With Effects of Digitization and Dead Time

In this experimental platform, the dc bus voltage can be considered ideal when the dc-side resistance R_1 is not introduced and the output power is not large. This group of experiments set up different carrier ratios N and dead time Δt to verify the superimposed effect of digitization and dead time.

The experimental waveforms and comparison results with N = 40 and 200 and $\Delta t = 2\ \mu$s and 5 μs are shown in Fig. 15(a)–(c), and due to space limitation, the phase comparisons of some experiments are omitted.

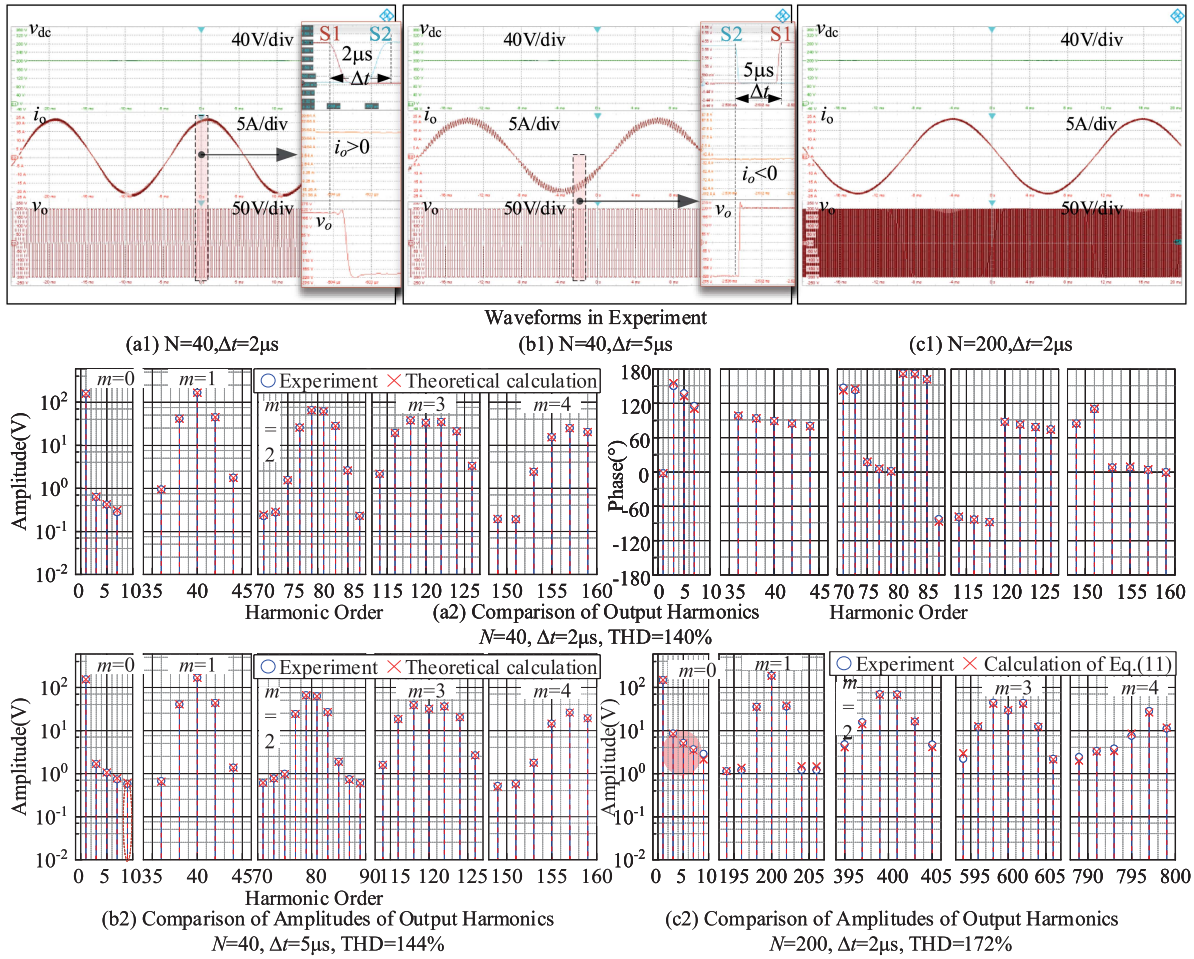

Fig. 15. Experimental waveforms and comparison of experimental and calculation results of output harmonic components without DC bus voltage oscillations. (a1) and (a2) Carrier ratio $N = 40$, $\Delta t = 2\,\mu$s. (b1) and (b2) Carrier ratio $N = 40$, $\Delta t = 5\,\mu$s. (c1) and (c2) Carrier ratio $N = 200$, $\Delta t = 2\,\mu$s.

By comparing Fig. 15(a2) and (b2) and (a2) and (c2), such as the third to ninth highlighted harmonic components and THD, it can be seen that the increase in dead time Δt and carrier ratio N both enlarge the harmonic amplitudes. From the previous group of experiments **a)**, it is clear that a large carrier ratio reduces the impact of digitization, so the increase in harmonic amplitudes in Fig. 15(c) proves that a large carrier ratio will significantly exacerbate the effects of dead time.

These conclusions are consistent with the analysis presented previously, while the amplitude and phase of experimental and theoretical calculations through (11) in the harmonic spectra Fig. 15(a2)–(c2) are agreeable, so the analysis of the dead time in this article can be verified.

C. Experimental Results With Effects of Digitization and DC Bus Voltage Oscillations

Since the switching duration exists in practice, the minimum dead time ($0.2\,\mu$s) is set, and the effect of dead time of this scale can be ignored.

The experimental results and comparison after introducing dc bus voltage oscillations are shown in Fig. 16. The driving signals of S_1 and S_2 and the amplified modulation process are illustrated in Fig. 16(b1), the harmonic distributions of dc bus voltage can be found in Table IV, and some representative output harmonic amplitudes are listed in Table V to further verify the accuracy of the proposed harmonic spectra.

Since the amplitudes of dc bus harmonic components in experiment are relatively small except for the second harmonic, the effects of the odd-order harmonic components in the dc bus is not obvious and can be seen only in a few output harmonic components such as dc component and 2nd, 5th, 19th, and 21st harmonic components in Fig. 16(a2), which are consistent with the previous analysis. The experimental results are in good agreement with the calculated results while the obtained dc bus harmonic components are substituted into the proposed spectrum (17) for calculation.

It can be noted that the smaller carrier ratio ($N = 20$) still makes the output harmonic components more significant in this group of experiments.

D. Experimental Results With Effects of Digitization, Dead Time and DC Bus Voltage Oscillations

This group of experiments considers the superimposed effects of three nonlinear factors commonly found in practical converter

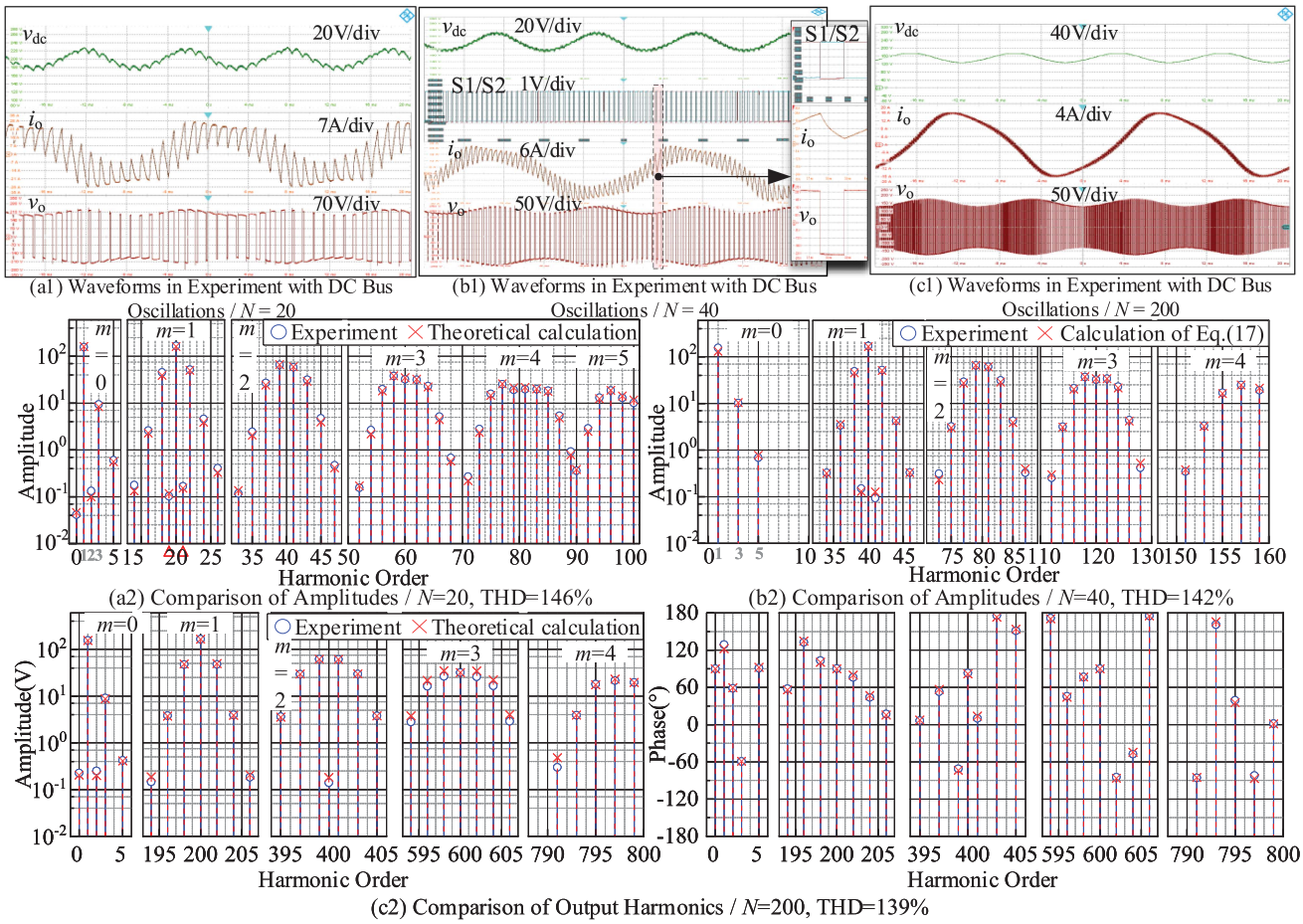

Fig. 16. Experimental waveforms and comparison of experimental and calculation results of output harmonic components with DC bus oscillations. (a1) and (a2) carrier ratio $N = 20$. (b1) and (b2) Carrier ratio $N = 40$. (c1) and (c2) Carrier ratio $N = 200$.

TABLE IV
DC BUS HARMONIC COMPONENTS DISTRIBUTIONS

Harmonic order			0	1	2	4	17	19	21	23	39	41
Amplitude (V)	Fig.16	N = 20	199	0.25	21.57	1.44	1	2.74	2.85	0.84		
		N = 40	199	0.24	26.32	1.93					1.2	1.27
		N = 200	198	0.25	22.69	1.02						
	Fig.17	N = 20, $\Delta t = 2\mu$s	199	0.2	22.23	1.5		2.83	2.92			
		N = 20, $\Delta t = 5\mu$s	199	0.27	21.3	1.83		2.82	2.92			
		N = 200, $\Delta t = 2\mu$s	198	0.2	22.6	1.03						

TABLE V
EXACT AMPLITUDES OF REPRESENTATIVE OUTPUT HARMONIC COMPONENTS IN EXPERIMENTS AND CALCULATIONS

Harmonic frequencies				0	ω_m	$2\omega_m$	$3\omega_m$	$\omega_c - 2\omega_m$	$\omega_c - \omega_m$	ω_c
Amplitude (V)	Fig.16	N = 40	Experiment	0.007	163.48	0.058	10.212	48.29	0.04	169.18
			Eq. (17)	0.006	164.41	0.06	10.424	47.47	0.02	169.03
		N = 200	Experiment	0.227	154.79	0.249	9.04	46.96	0.017	164.1
			Eq. (17)	0.204	153.95	0.2	8.718	48	0.02	164.53
	Fig.17	N = 200, $\Delta t = 2\mu s$	Experiment	0.128	144.38	0.337	8.57	45.46	0.16	173.22
			Eq. (20)	0.125	144.14	0.376	8.81	45.92	0.11	174.56

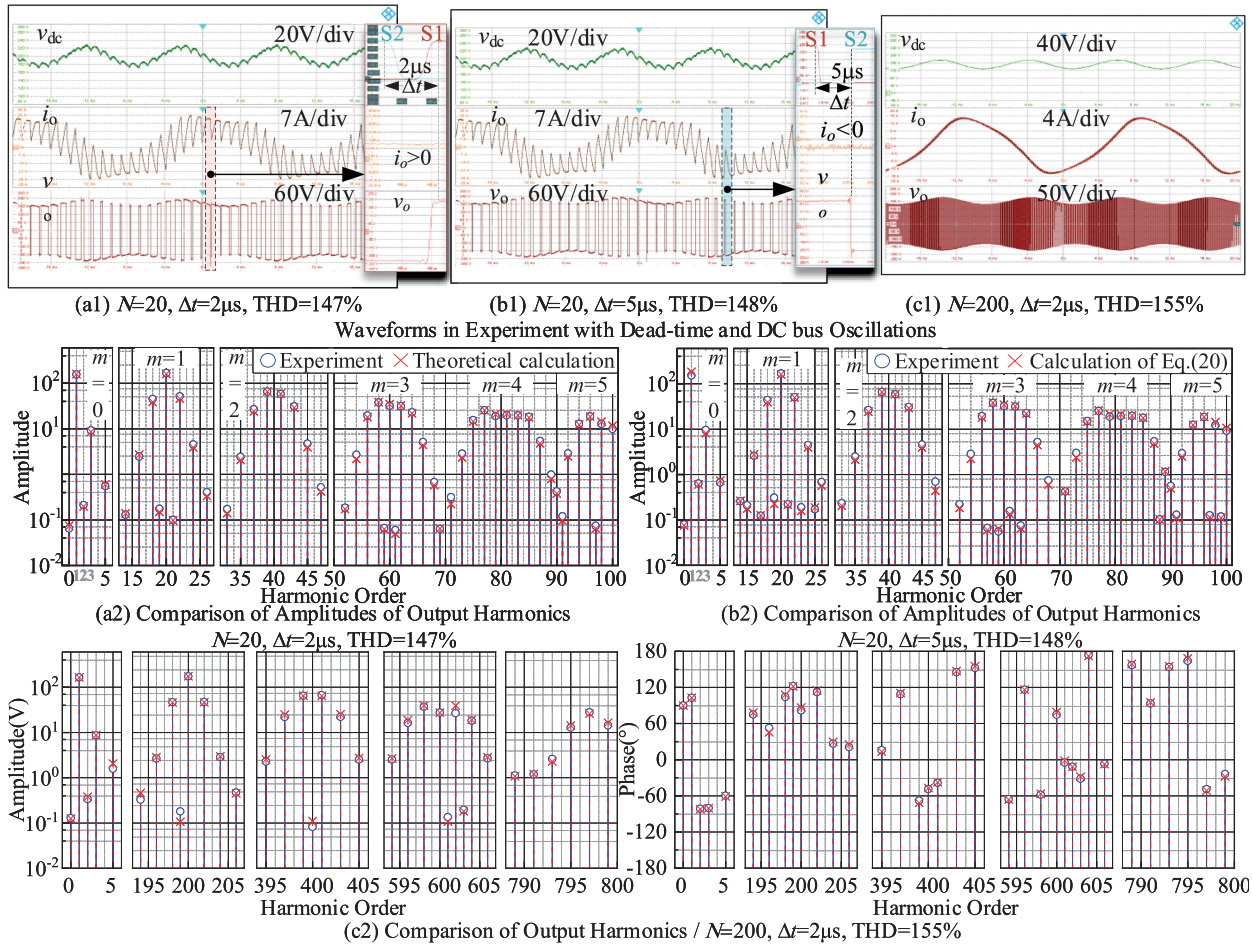

Fig. 17. Experimental waveforms and comparison of experimental and calculation results of output harmonic components with dead time and DC bus oscillations. (a1) and (a2) $N = 20$, $\Delta t = 2\,\mu$s. (b1) and (b2) $N = 20$, $\Delta t = 5\,\mu$s. (c1) and (c2) $N = 200$, $\Delta t = 2\,\mu$s.

systems. The experimental waveforms and results with different dead time Δt are shown in Fig. 17, where the dc bus harmonic distributions are listed in Table IV.

The effects of dead time on the output voltage can be obtained in Fig. 17(a1) and (b1) for opposite polarity of output current i_o, which is consistent with the analysis in Section II.

In the output harmonic distribution in Fig. 17(a2) to (c2), the dc component and second, third, and fifth baseband harmonic components introduced by first, second, and fourth dc bus harmonic components can be found in m=0 group; and the sideband harmonic components introduced by odd-order dc bus harmonic components (1st, 19th, and 21st) near carrier harmonic components with the same parity (e.g., $\omega_c - \omega_m$ near group of $m = 1$ and $3\omega_c + \omega_m$ near group of $m = 3$), which are more visible when the dead time is increased in Fig. 17(b2).

More importantly, the results of the theoretical calculation by substituting the dc bus harmonic components into the proposed spectrum (20) are almost identical to the experimental results.

It is worth noting that in Figs. 16(a1) and (b1) and 17(a1) and (b1), the current waveform shows significant ripple and distortion. This is because the addition of the dc-side resistor increases the dc bus voltage harmonic components (listed in Table IV), while these experiments are at low switching frequencies (1 and 2 kHz). From the combined effects analyzed in Section V, it is clear that the effects of both dc bus voltage ripple and digitization will be enhanced at this time, resulting in significant harmonic components of output. When the switching frequency increases, as shown in Figs. 16(c1) and 17(c1), the effect of digitization is significantly reduced with $N = 200$, and the current ripple almost disappears; however, the distortion caused by the dc bus voltage ripple still exists.

The previous analysis on the combined effect of nonlinear factors can be verified from the variation of current with carrier ratio in Figs. 16 and 17.

Through the aforementioned four groups of experiments, the correctness of the analytical solution of output harmonic and the accuracy of harmonic spectra proposed in this article can be verified. And the proposed combined effect of the nonlinear factors is also verified.

VII. Conclusion

This article establishes a digitally controlled H-bridge VSI model that is closer to practical application, and then, analyzes the mechanism of output voltage harmonic components generation based on the modulation process of PWM. Thus, an analytical solution of the output voltage harmonic spectrum

that can be easily extended to a wide range of applications is proposed.

The individual and combined effects of the three major nonlinear factors—digitization, dead time, and dc bus voltage ripple presented in the actual system are analyzed and summarized by this solution, and these output spectra are given in a precise manner. The correctness and feasibility of the presented results are demonstrated by simulations and experiments .

APPENDIX

A. Time-Domain Expression of the Ideal Modulation and Carrier Waveforms in Each 2π Carrier Period

$$u_{im} = U_m \sin y$$
$$u_c = \begin{cases} -\frac{2}{\pi}U_c(x+\frac{\pi}{2}) & -\pi \le x \le 0 \\ \frac{2}{\pi}U_c(x-\frac{\pi}{2}) & 0 < x \le \pi. \end{cases} \tag{A1}$$

B. Time-Domain Expression of the Ideal Output Voltage in Each 2π Carrier Period

$$v_o = \begin{cases} -v_{\rm dc} & -\pi \le x < X_f \\ v_{\rm dc} & X_f \le x \le X_r \\ -v_{\rm dc} & X_r < x \le \pi. \end{cases} \tag{A2}$$

C. Specific Solution Procedure for the Coefficients of the Analytical Ideal Output Voltage Harmonic Spectrum

$$\begin{aligned} C_{mn}^0 &= A_{mn}^0 + jB_{mn}^0 = \frac{\mathrm{V_{dc}}}{2\pi^2}\cdot \\ &= \Bigg(-\int_{-\pi}^{\pi}\int_{-\pi}^{-\frac{\pi}{2}(1+M\sin y)} e^{j(mx+ny)}dxdy \\ &+ \int_{-\pi}^{\pi}\int_{-\frac{\pi}{2}(1+M\sin y)}^{\frac{\pi}{2}(1+M\sin y)} e^{j(mx+ny)}dxdy \\ &- \int_{-\pi}^{\pi}\int_{\frac{\pi}{2}(1+M\sin y)}^{\pi} e^{j(mx+ny)}dxdy \Bigg) \end{aligned} \tag{A3}$$

D. General Form of the Output Voltage Harmonic Spectrum in SPWM

It can be divided into the dc component, fundamental and baseband harmonic components, carrier harmonic components, and sideband harmonic components.

$$\begin{aligned} v_o = \frac{C_{00}}{2} &+ \mathrm{Re}\sum_{n=1}^{\infty} C_{0n}e^{-jny} + \mathrm{Re}\sum_{m=1}^{\infty} C_{m0}e^{-jmx} \\ &+ \mathrm{Re}\sum_{m=1}^{\infty}\sum_{n=\pm 1}^{\pm\infty} C_{mn}e^{-j(mx+ny)} \end{aligned} \tag{A4}$$

where Re represents the real part of a complex number.

E. Time-Domain Expression of the Output Voltage With Dead Time

$$v_o = \begin{cases} \begin{cases} -v_{dc} & -\pi \le x < X_f+\omega_c t_{off} \\ v_{dc} & X_f+\omega_c t_{off} \le x \le X_r+\omega_c t_d \\ -v_{dc} & X_r+\omega_c t_d < x \le \pi \end{cases} \\ -\pi+\varphi_i \le y \le \varphi_i; \\ \begin{cases} -v_{dc} & -\pi \le x < X_f+\omega_c t_d \\ v_{dc} & X_f+\omega_c t_d \le x \le X_r+\omega_c t_{off} \\ -v_{dc} & X_r+\omega_c t_{off} < x \le \pi \end{cases} \\ \varphi_i \le y < \varphi_i+\pi; \end{cases} \tag{A5}$$

F. Half-Periodic Integral Calculation of Double Fourier Series Coefficients for Output Voltage With Dead Time

$$\begin{aligned} C_{mn}^0 &= A_{mn}^0 + jB_{mn}^0 = \frac{\mathrm{V_{dc}}}{2\pi^2}\cdot \\ &\Bigg(-\int_{-\pi+\varphi_i}^{\varphi_i}\int_{-\pi}^{-\frac{\pi}{2}(1+M\sin y)+\varphi_c+\omega_c t_{off}} \\ &\quad e^{j(mx+n(y+\frac{x+\pi-\varphi_c}{N}))}dxdy \\ &+ \int_{-\pi+\varphi_i}^{\varphi_i}\int_{-\frac{\pi}{2}(1+M\sin y)+\varphi_c+\omega_c t_{off}}^{0} \\ &\quad e^{j(mx+n(y+\frac{x+\pi-\varphi_c}{N}))}dxdy \\ &+ \int_{-\pi+\varphi_i}^{\varphi_i}\int_{0}^{\frac{\pi}{2}(1+M\sin y)+\varphi_c+\omega_c t_d} e^{j(mx+n(y+\frac{x-\varphi_c}{N}))}dxdy \\ &- \int_{-\pi+\varphi_i}^{\varphi_i}\int_{\frac{\pi}{2}(1+M\sin y)+\varphi_c+\omega_c t_d}^{\pi} e^{j(mx+n(y+\frac{x-\varphi_c}{N}))}dxdy \\ &- \int_{\varphi_i}^{\pi+\varphi_i}\int_{-\pi}^{-\frac{\pi}{2}(1+M\sin y)+\varphi_c+\omega_c t_d} e^{j(mx+n(y+\frac{x+\pi-\varphi_c}{N}))}dxdy \\ &+ \int_{\varphi_i}^{\pi+\varphi_i}\int_{-\frac{\pi}{2}(1+M\sin y)+\varphi_c+\omega_c t_d}^{0} e^{j(mx+n(y+\frac{x+\pi-\varphi_c}{N}))}dxdy \\ &+ \int_{\varphi_i}^{\pi+\varphi_i}\int_{0}^{\frac{\pi}{2}(1+M\sin y)+\varphi_c+\omega_c t_{off}} e^{j(mx+n(y+\frac{x-\varphi_c}{N}))}dxdy \\ &- \int_{\varphi_i}^{\pi+\varphi_i}\int_{\frac{\pi}{2}(1+M\sin y)+\varphi_c+\omega_c t_{off}}^{\pi} e^{j(mx+n(y+\frac{x-\varphi_c}{N}))}dxdy \Bigg) \end{aligned} \tag{A6}$$

G. Example of the Application of the Proposed Spectrum: The Calculation of Optimal Dead Time

As mentioned before, the accurate harmonic spectrum proposed in this article can be used as a theoretical basis for parameter design or harmonic compensation, and the calculation of optimal dead time will be taken as an example to illustrate.

The calculation flow of the optimal dead time is as follows.

1) Determine the system parameters: carrier ratio, modulation ratio, fundamental frequency, etc.
2) Select the undesired harmonic components to be reduced (e.g., third and fifth harmonic components or THD, taking third harmonic component as an example).
3) Calculate the expression of this undesired harmonic component in the proposed harmonic spectrum (20). And the expression of the third harmonic component can be seen as the sum of (23) and (24) in Section V.

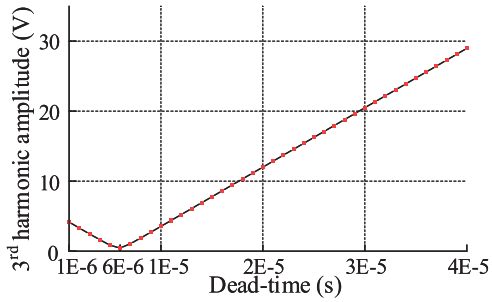

Fig. 18. Amplitude of the third harmonic component under different dead time.

4) Calculate the amplitude of the selected harmonic component in different cases with dead time as a variable. The example of the third harmonic component is shown in Fig. 18.
5) The dead time (6×10^{-6}s) with the minimal harmonic amplitude is selected as optimal within the tolerable range of the actual device.

H. Extension to the Unipolar Modulation Strategy With Digitization

The output voltage in unipolar modulation can be equated to the difference of two bipolar modulation output voltages (v_P–v_N) with opposite modulation waveforms and half the dc bus voltage. For the output voltage v_P under positive modulation waveform, we can directly substitute $0.5v_{\rm dc}$ into the expression presented in this article. When the modulation waveform is reversed, its intersection point with the carrier wave will be changed as

$$\begin{cases} X_{r\rm N} = \frac{\pi}{2}\left(1 - M\sin y\right) + \varphi_c + 2p\pi \\ X_{f\rm N} = -\frac{\pi}{2}\left(1 - M\sin y\right) + \varphi_c + 2p\pi \end{cases} \tag{A7}$$

Except for the intersection points and dc bus voltage, the analysis process in v_N is consistent with this article, including the digitization process. Therefore, we can obtain the coefficients of the double Fourier series expansion and the final harmonic spectrum of the output voltage v_N in a similar manner, thus obtaining the complete output voltage spectrum.

$$v_{o\_u}^0 = \mathrm{Re}\frac{4jV_{dc}}{\pi}\left(\sum_{n=1,3,5\ldots}^{+\infty}\frac{N}{n}J_n\left(\frac{nM\pi}{2N}\right)e^{j\frac{n\pi}{2N}}e^{-jny}\right.$$
$$\left.+\sum_{m=2,4,6\ldots}^{+\infty}\sum_{n=\pm1,\pm3\ldots}^{\pm\infty}\frac{1}{\alpha}\cos\frac{m\pi}{2}J_n\left(\xi\right)e^{j\left(\frac{n\pi}{2N}+m\varphi_c\right)}e^{-j(mx+ny)}\right) \tag{A8}$$

REFERENCES

[1] G. Li, J. Xia, K. Wang, Y. Deng, X. He, and Y. Wang, "Hybrid modulation of parallel-series LLC resonant converter and phase shift full-bridge converter for a dual-output DC-DC converter," *IEEE Trans. Emerg. Sel. Topics Power Electron.*, vol. 7, no. 2, pp. 833–842, Jun. 2019.

[2] S. Kouro et al., "Recent advances and industrial applications of multilevel converters," *IEEE Trans. Ind. Electron.*, vol. 57, no. 8, pp. 2553–2580, Aug. 2010.

[3] G. Grandi, J. Loncarski, and O. Dordevic, "Analysis and comparison of peak-to-peak current ripple in two-level and multilevel PWM inverters," *IEEE Trans. Ind. Electron.*, vol. 62, no. 5, pp. 2721–2730, May 2015.

[4] S. Wang, G. P. Adam, A. M. Massoud, D. Holliday, and B. W. Williams, "Analysis and assessment of modular multilevel converter internal control schemes," *IEEE Trans. Emerg. Sel. Topics Power Electron.*, vol. 8, no. 1, pp. 697–719, Mar. 2020.

[5] M. A. Perez, S. Bernet, J. Rodriguez, S. Kouro, and R. Lizana, "Circuit topologies, modeling, control schemes, and applications of modular multilevel converters," *IEEE Trans. Power Electron.*, vol. 30, no. 1, pp. 4–17, Jan. 2015.

[6] B. Gao, Y. Liu, B. Shao, and H. Ran, "A path analysis method to study the subsynchronous oscillation mechanism in direct-drive wind farm with VSC-HVDC system," *Int. J. Elect. Power Energy Syst.*, vol. 142, pp. 108328–108341, 2022.

[7] J. Fu, L. Chen, H. Zhao, and P. Zhang, "High and low frequency control strategy for APF DC side ripple voltage under unbalanced load," in *Proc. IEEE 2nd Int. Conf. Electron. Commun. Eng.*, 2019, pp. 326–330.

[8] R. Wang, W. Huang, B. Hu, Q. Du, and X. Guo, "Harmonic detection for active power filter based on two-step improved EEMD," *IEEE Trans. Instrum. Meas.*, vol. 71, 2022, Art. no. 9001510.

[9] J. A. Sontakke and G. Choudhary, "Design of digital controller using pole placement technique for single phase PWM inverter and its implementation on FPGA," in *Proc. Int. Conf. Nascent Technol. Eng.*, 2017, pp. 1–7.

[10] D. Gillard, T. Cameron, A. Prochazka, and M. Gauthier, "Tremor suppression using functional electrical stimulation: A comparison between digital and analog controllers," *IEEE Trans. Rehabil. Eng.*, vol. 7, no. 3, pp. 385–388, Sep. 1999.

[11] B. Patella, A. Prodic, A. Zirger, and D. Maksimovic, "High-frequency digital PWM controller IC for DC-DC converters," *IEEE Trans. Power Electron.*, vol. 18, no. 1, pp. 438–446, Jan. 2003.

[12] S. Bibian and H. Jin, "High performance predictive dead-beat digital controller for DC power supplies," *IEEE Trans. Power Electron.*, vol. 17, no. 3, pp. 420–427, May 2002.

[13] D. C. Moore, M. Odavic, and S. M. Cox, "Dead-time effects on the voltage spectrum of a PWM inverter," *IMA J. Appl. Math.*, vol. 79, no. 6, pp. 1061–1076, 2014.

[14] J.-W. Choi and S.-K. Sul, "Inverter output voltage synthesis using novel dead time compensation," *IEEE Trans. Power Electron.*, vol. 11, no. 2, pp. 221–227, Mar. 1996.

[15] S.-H. Hwang and J.-M. Kim, "Dead time compensation method for voltage-fed PWM inverter," *IEEE Trans. Energy Convers.*, vol. 25, no. 1, pp. 1–10, Mar. 2010.

[16] F. Blaabjerg, D. Neacsu, and J. Pedersen, "Adaptive SVM to compensate DC-link voltage ripple for four-switch three-phase voltage-source inverters," *IEEE Trans. Power Electron.*, vol. 14, no. 4, pp. 743–752, Jul. 1999.

[17] Q. Tu, Z. Xu, Y. Chang, and L. Guan, "Suppressing DC voltage ripples of MMC-HVDC under unbalanced grid conditions," *IEEE Trans. Power Del.*, vol. 27, no. 3, pp. 1332–1338, Jul. 2012.

[18] W. R. Bennett, "New results in the calculation of modulation products," *Bell Syst. Tech. J.*, vol. 12, no. 2, pp. 228–243, 1933.

[19] H. d. T. Mouton, B. McGrath, D. G. Holmes, and R. H. Wilkinson, "One-dimensional spectral analysis of complex PWM waveforms using superposition," *IEEE Trans. Power Electron.*, vol. 29, no. 12, pp. 6762–6778, Dec. 2014.

[20] B. McGrath and H. d. T. Mouton, "One-dimensional spectral analysis techniques for multilevel PWM strategies," *IEEE Trans. Power Electron.*, vol. 31, no. 10, pp. 6910–6919, Oct. 2016.

[21] Z. Yonghui, C. Xi, and Z. Xiyuan, "Power harmonic analysis based on all-phase FFT1," in *Proc. 2nd Int. Conf. Signal Process. Syst.*, 2010, vol. 3, pp. 576–579.

[22] H. Wen, Z. Teng, Y. Wang, B. Zeng, and X. Hu, "Simple interpolated FFT algorithm based on minimize sidelobe windows for power-harmonic analysis," *IEEE Trans. Power Electron.*, vol. 26, no. 9, pp. 2570–2579, Sep. 2011.

[23] F. Zhang, Z. Geng, and W. Yuan, "The algorithm of interpolating windowed FFT for harmonic analysis of electric power system," *IEEE Trans. Power Del.*, vol. 16, no. 2, pp. 160–164, Apr. 2001.

[24] I. Deslauriers, N. Avdiu, and B. T. Ooi, "Naturally sampled triangle carrier PWM bandwidth limit and output spectrum," *IEEE Trans. Power Electron.*, vol. 20, no. 1, pp. 100–106, Jan. 2005.

[25] R. H. Wilkinson, T. A. Meynard, and H. du Toit Mouton, "Natural balance of multicell converters: The two-cell case," *IEEE Trans. Power Electron.*, vol. 21, no. 6, pp. 1649–1657, Nov. 2006.

[26] R. H. Wilkinson, T. A. Meynard, and H. du Toit Mouton, "Natural balance of multicell converters: The general case," *IEEE Trans. Power Electron.*, vol. 21, no. 6, pp. 1658–1666, Nov. 2006.
[27] D. G. Holmes and T. A. Lipo, *Pulse Width Modulation for Power Converters: Principles and Practice*. Hoboken, NJ, USA:Wiley-IEEE Press, Oct. 2003.
[28] J.-W. Jung and M. Hawksford, "An oversampled digital PWM linearization technique for digital-to-analog conversion," *IEEE Trans. Circuits Syst.*, vol. 51, no. 9, pp. 1781–1789, Sep. 2004.
[29] M. Kumar and R. Gupta, "Sampling effect characterization of digital SPWM of VSI in time domain," *IEEE Trans. Ind. Electron.*, vol. 63, no. 7, pp. 4150–4159, Jul. 2016.
[30] J. Ye, S. Huang, L. Liu, L. Li, J. Xu, and A. Shen, "Accurate harmonic calculation for digital SPWM of VSI with dead-time effect," *IEEE Trans. Power Electron.*, vol. 36, no. 7, pp. 7892–7902, Jul. 2021.
[31] M. Kumar, "Time-domain characterization of digitized PWM inverter with dead-time effect," *IEEE Trans. Circuits Syst.*, vol. 65, no. 10, pp. 3592–3601, Oct. 2018.
[32] N. Jiao, S. Wang, T. Liu, Y. Wang, and Z. Chen, "Harmonic quantitative analysis for dead-time effects in SPWM inverters," *IEEE Access*, vol. 7, pp. 43143–43152, 2019.
[33] A. Tcai, I. M. Alsofyani, and K.-B. Lee, "DC-link ripple reduction in a DPWM-based two-level VSC," in *Proc. IEEE Energy Convers. Congr. Expo.*, 2018, pp. 1483–1487.
[34] S. Kouro, P. Lezana, M. Angulo, and J. Rodriguez, "Multicarrier PWM with DC-link ripple feedforward compensation for multilevel inverters," *IEEE Trans. Power Electron.*, vol. 23, no. 1, pp. 52–59, Jan. 2008.
[35] C. D. Townsend, T. J. Summers, and R. E. Betz, "Impact of practical issues on the harmonic performance of phase-shifted modulation strategies for a cascaded H-bridge StatCom," *IEEE Trans. Ind. Electron.*, vol. 61, no. 6, pp. 2655–2664, Jun. 2014.
[36] S. Milovanovic and D. Dujic, "Comprehensive spectral analysis of PWM waveforms with compensated DC-link oscillations," *IEEE Trans. Power Electron.*, vol. 35, no. 12, pp. 12898–12908, Dec. 2020.
[37] S. S. Thakur, M. Odavic, A. Allu, Z. Q. Zhu, and K. Atallah, "Theoretical harmonic spectra of PWM waveforms including DC bus voltage ripple—Application to a low-capacitance modular multilevel converter," *IEEE Trans. Power Electron.*, vol. 35, no. 9, pp. 9291–9305, Sep. 2020.

Haozhe Wang was born in Hubei Province, China, in 1997. He received the B.S. degree in Automation from the School of Artificial Intelligence and Automation, Huazhong University of Science and Technology, Wuhan, China, in 2019, where he is currently working toward the Ph.D. degree in control science and engineering.

His research interests include power electronics, harmonics suppression, circuit theory, and stability analysis.

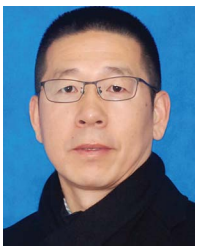

Jinbang Xu was born in Hubei, China, in 1973. He received the Ph.D. degree in control science and engineering from the Department of Control Science and Engineering, Huazhong University of Science and Technology (HUST), Wuhan, China, in 2004.

He is currently a professional with the School of Automation, HUST. His research interests include power electronics, intelligent control, and smart grid.

Jie Ye was born in Hubei Province, China, in 1989. He received the B.S. degree in software engineering from the Department of Software Engineering, Xidian University, Xian, China, in 2011, and the Ph.D. degree in control science and engineering from the School of Artificial Intelligence and Automation, Huazhong University of Science and Technology, Wuhan, China, in 2017.

He is currently working as an Associate Professor with the Huazhong University of Science and Technology. His research interests include signal processing, circuit theory, harmonics suppression, and reactive power compensation.

Baojin Li was born in Anhui Province, China, in 1992. He received the B.S. degree in automation from the Department of Electronic Information and Electrical Engineering, Dalian University of Technology, Dalian, China, in 2016. He is currently working toward the Ph.D. degree in control science and engineering with the School of Artificial Intelligence and Automation, Huazhong University of Science and Technology, Wuhan, China.

His current research interests include power electronics, harmonics suppression, and circuit theory.

Songtao Huang (Student Member, IEEE) was born in Hubei Province, China, in 1994. He received the B.S. degree in control science and engineering from the School of Control Science and Engineering, Shandong University, Shandong, China, in 2017. He is currently working toward the Ph.D. degree in control science and engineering with the School of Artificial Intelligence and Automation, Huazhong University of Science and Technology, Wuhan, China.

His research interests include power electronics, dead-time effect, harmonics suppression, and optimization algorithms.

Yukai Huang was born in Henan Province, China, in 1998. He received the B.S. degree in automation from the School of Artificial Intelligence and Automation, Huazhong University of Science and Technology, Wuhan, China, in 2020, where he is currently working toward the Ph.D. degree in control science and engineering.

His research interests include power electronics, dead-time effect, harmonics suppression, and modern control theory.

Dong Liu received the B.E. degree in automation from the School of Artificial Intelligence and Automation, Huazhong University of Science and Technology, Wuhan, China, in 2020, where he is currently working toward the Ph.D. degree in control science and engineering.

His research interests include distributed optimization in multiagent systems, virtual power plants, and repetitive controllers in active power plant.

Anwen Shen (Member, IEEE) received the B.S. and M.S. degrees in automation from Zhejiang University, Zhejiang, China, in 1991 and 1994, respectively, and the Ph.D. degree in automation from the Huazhong University of Science and Technology (HUST), Wuhan, China, in 1997.

In 1997, he joined the Department of Control Science and Engineering, HUST, where he is currently working as a Professor with the School of Automation. He is a holder of more than ten patents. His research interests include advanced motion control, power electronic applications, motor drives, electrical vehicles, and intelligent control.